The Thesis Committee for Ziad Abdullrahman Alabdullatif
Certifies that this is the approved version of the following thesis:

Analysis of Downhole Drilling Vibrations:

Case Studies of Manifa and Karan Fields in Saudi Arabia

Approved by
Supervising Committee:

Supervisor: _____

Kenneth E. Gray

_____

Fred Florence

Analysis of Downhole Drilling Vibrations:

Case Studies of Manifa and Karan Fields in Saudi Arabia

by

Ziad Abdullrahman Alabdullatif, B.S.

Thesis

Presented to the Faculty of the Graduate School of

The University of Texas at Austin

in Partial Fulfillment

of the Requirements

for the Degree of

Master of Science in Engineering

The University Of Texas At Austin

August 2011

Dedication

To my family

Acknowledgements

First and foremost, I would like to express my utmost gratitude to my supervisor **Dr. Ken Gray** for his support during my years of study. I am glad that I was accepted at the “Life-of-Well: Rock, Fluid, and Stress Systems” research program. This program provided me with the guidance, knowledge, and experience that helped me in writing my MS Thesis.

I am also deeply grateful to **Fred Florence** for his efforts and contribution as part of the thesis committee.

I would like to thank **Saudi Aramco** for providing me a scholarship and for permission to publish this work.

I owe a debt of gratitude to **National Oilwell Varco (NOV)** for their cooperation and help in using Vibrascope™. I am very thankful to **Fred Florence** and **Bill Koederitz** for their support. A special thank goes to **Chris Hanley** whose tutorial on Vibrascope™ was very knowledgeable for me. His help in running different BHA harmonic designs was of great value.

Finally, I owe much to my family: my parents **Abdulrahman** and **Badreyah**. This work would not be accomplished without their never-ending love, encouragement and support throughout my life. I also would like to express my sincere thanks to my little sisters and brothers for cheering me up during my study.

August 12, 2011

Abstract

Analysis of Downhole Drilling Vibrations:

Case Studies of Manifa and Karan Fields in Saudi Arabia

Ziad Abdullrahman Alabdullatif, M.S.E.

The University of Texas at Austin, 2011

Supervisor: Kenneth E. Gray

Downhole vibrations lead to downhole failures and decrease the rate of penetration (ROP). The bottom hole assembly (BHA) static and dynamic design is a key factor in optimizing drilling operations. The BHA should be designed to minimize the vibration levels in the axial, lateral, and torsional directions. This would be achieved by avoiding rotating the drillstring in the speeds that are nearby the natural frequency of BHA. The complexity associated with current BHA components requires using advanced computational tools that are capable of solving complex and time-consuming equations. Finite Element Analysis (FEA) is the most used technique in analyzing vibration behavior of the drillstring by mesh discretizing of a continuous body into small elements. This thesis will study

the dynamic behavior of different BHA designs for Manifa and Karan fields of Saudi Aramco to optimize the drilling operations. The FEA software that will be used to conduct these studies is called Vibrascope™, which was developed by NOV. The software will determine the critical speeds of the drillstring that should be avoided to prevent resonance of the BHA, which will lead to severe downhole vibration.

TABLE OF CONTENTS

LIST OF TABLES

LIST OF FIGURES

1. INTRODUCTION

Drilling wells is becoming more complex while the demand for extended reach and/or directional/horizontal drilling is increasing (Bailey et al. 2008; Ledgerwood et al. 2010). Downhole vibrations of drillstring in rotary drilling have been recognized as one of the most significant factors contributing to operational problems. Drilling vibration modes are axial, lateral, and torsional (Rajnauth and Jagai 2003). In axial vibrations, the bit is bounced up and down and often occurs in hard formations (Shuttleworth et al. 1998; Dupriest et al. 2005). Lateral vibration occurs when the motion is perpendicular to the drillstring leading to bending and BHA whirl (Shuttleworth et al. 1998; Dupriest et al. 2005). Torsional vibration is a twisting motion that causes the surface torque to fluctuate, which can generate stick-slip motion at extreme cases (Shuttleworth et al. 1998; Rajnauth and Jagai 2003). Bailey et al. (2008) estimated that 40% out of the 4 million footage drilled by ExxonMobil annually was affected by downhole vibration. The operational problems associated with vibrations include decrease in ROP and footage improvements, pre-mature failure of drilling components such as Rotary Steerable (RSS) or Logging While Drilling (LWD), pre-mature bit failure, drillstring fatigue, poor control of directional tools, sidetracking or fishing due to downhole break, and in the worst case, well abandonment (Macpherson et al. 1993; Rajnauth and Jagai 2003; Bailey et al. 2008).

The number of research papers that discuss vibrations control has increased in recent years due to advancement in downhole measurements and

computing capabilities (Bailey et al. 2008). Analyzing Bottom Hole Assembly (BHA) design of the drillstring prior to drilling is an essential step. Optimized BHA design that decreases the vibrations will have positive economical and environmental impacts. Every drilling application has its BHA design criteria. For example, drilling a soft formation in shallow depths requires a different BHA design from drilling a hard formation at the same depth.

Prior to drilling, lateral, axial, and torsional vibrations need to be carefully analyzed to avoid resonance (Macpherson et al. 1993; Craig et al. 2009). Resonance is defined as the tendency of a system to oscillate at maximum amplitude at certain frequencies called “natural frequencies” (Macpherson et al. 1993; Craig et al. 2009). Thus, rotating the drillstring in a speed that is close to the BHA critical speed would lead the system to resonate and, consequently, results in severe downhole vibration (Craig et al. 2009). In other words, the frequency of rotating the drill string should not be close to the natural frequency of the BHA to avoid resonance. Macpherson et al. (1993) state that the drillstring may still exhibit high vibration levels even if the system is not close to the natural frequency if high level of excitation sources is present .

This thesis investigates and analyzes dynamic BHA designs for Manifa and Karan fields of Saudi Aramco using a software package to study the vibration modes and their severity. The goal of this study is reducing the high well cost and optimize drilling operations associated with Manifa and Karan development projects. Vibrascope™, developed by National Oil Varco Company

(NOV), is a drillstring dynamics modeling software tool that uses finite element analysis approach (FEA) (Craig et al. 2009). For complicated systems such as the drillstring, Finite Element Analysis (FEA) is used to solve complex and time-consuming equations (Craig et al. 2009). FEA breaks the complex system into smaller parts so that the analytical solution could be achieved easily and accurately (Craig et al. 2009). Each part represents a finite piece that has its own characteristics such as material properties (Craig et al. 2009). Vibrascope™ enables pre-well analysis of the BHA and drillstring by calculating the harmonic frequencies in axial, lateral and torsional direction (Craig et al. 2009). The software will predict the rotary table speed per minute (RPM) at a certain weight on bit (WOB) that would result in resonance of the drillstring system in all directions from different excitation sources (Craig et al. 2009). The required inputs to analyze the model are string geometry and material, borehole geometry, 3D well path, WOB, and mud weight (Craig et al. 2009).

The thesis is organized as follows:

Chapter 2: Provides an overview about previous work in vibration modeling and the basics behind the BHA design.

Chapter 3: Presents dynamic analysis of extended reach wells drilled in Manifa oil field. The chapter will include study of vibration severity levels associated with the current design for critical hole sections.

Chapter 4: Offers dynamic study of critical hole sections for gas wells drilled in Karan offshore field.

Appendices: Provide extra information in different BHA design criteria.

2. LITERATURE REVIEW

2.1. Vibration Theory

Vibration responses are classified into (1) self-excitation vibration and (2) forced vibration (Zamudio et al. 1987). In a self-excited vibration, the alternating force that keeps the motion is created by the motion itself and will vanish when the motion stops (Piersol and Paez 2010). On the other hand, in a forced vibration, the external force is independent of the motion and will last when the motion stops (Zamudio et al. 1987; Piersol and Paez 2010).

For self-excited vibrations, the vibration level is affected by the excitation severity level, the system damping, and the closeness of the excitation frequency to the natural frequency of the drillstring (Macpherson et al. 1993).

Many physical sources excite the drillstring while drilling leading to vibration (Besaisow and Payne 1988; Macpherson et al. 1993). Table 2.1 summarizes different excitation mechanisms studied by Besaisow and Payne. It should be noted that a primary excitation force in a certain direction may lead to other secondary force(s) in the other directions (Besaisow and Payne 1988).

Table 2.1 Primary and secondary excitation mechanisms (Besaisow and Payne 1988)

Physical Mechanism	Primary Excitation	Secondary Excitation
Mass imbalance or bent pipe	$1 \times \omega$ lateral	$2 \times \omega$ axial $2 \times \omega$ torsional $2 \times \omega$ lateral
Misalignment	$1 \times \omega$ lateral $2 \times \omega$ lateral	$2 \times \omega$ axial $2 \times \omega$ axial
Three-cone bit	$3 \times \omega$ axial	$3 \times \omega$ torsional $3/2 \times \omega$ lateral
Very soft formation, low WOB, causing a loose drillstring	1, 2, 3, 4, and $5 \times \omega$ axial, torsional, and lateral	
Rotational walk (precessional, backward whirl)	$\left(\frac{d_h}{d_h - d_d}\right)\omega$ lateral	$2\left(\frac{d_h}{d_h - d_d}\right)\omega$ axial
		$2\left(\frac{d_h}{d_h - d_d}\right)\omega$ torsional
	$\frac{d_d}{d_h - d_d} \times \omega$ lateral	$2\frac{d_d}{d_h - d_d} \times \omega$ axial
		$2\frac{d_d}{d_h - d_d} \times \omega$ torsional
Nonsynchronous walk or whirl (experimental)	(0.8 to 1.0)$\frac{d_h}{d_h - d_d} \times \omega$ lateral	(1.6 to 2.0) $\times \frac{d_h}{d_h - d_d} \times \omega$ axial
	(1.6 to 2.0)$\left(\frac{d_h}{d_h - d_d} \times \omega\right)$	(1.6 to 2.0) $\times \frac{d_h}{d_h - d_d} \times \omega$ torsional
Drillstring whip (forward whirl)	ω harmonics ($1 \times \omega$, $2 \times \omega$, and $3 \times \omega$) lateral	ω harmonics (axial, torsional)

Mass imbalance is found to be one of the most important physical sources that induce excitation in the lateral mode by a magnitude of 1 x ω from a fixed reference frame (Besaisow and Payne 1988). Lateral vibration (bit eccentricity) results in significant decline in ROP even if the vibration level is small (Dupriest et al. 2005). Detecting lateral vibrations by the driller is hard because they are not

transmitted to the surface (Shuttleworth et al. 1998). Dykstra el al. (1996) conducted a laboratory test to study the effect of changing the rotary speed on the deflection amplitude from the center of the hole. They found that deflection magnitude increased gradually with the increase in the rotary speed as it is shown in Figure 2.1. When the rotary speed approaches the critical speed of the BHA, the deflection of the BHA from the center of the borehole increases sharply, which will indicate whirl due to the centrifugal force resulted from the eccentricity of the drill collar (Dykstra et al. 1996). Then, the deflection level will decrease sharply after passing the critical speed region indicating a safe range of rotary speed.

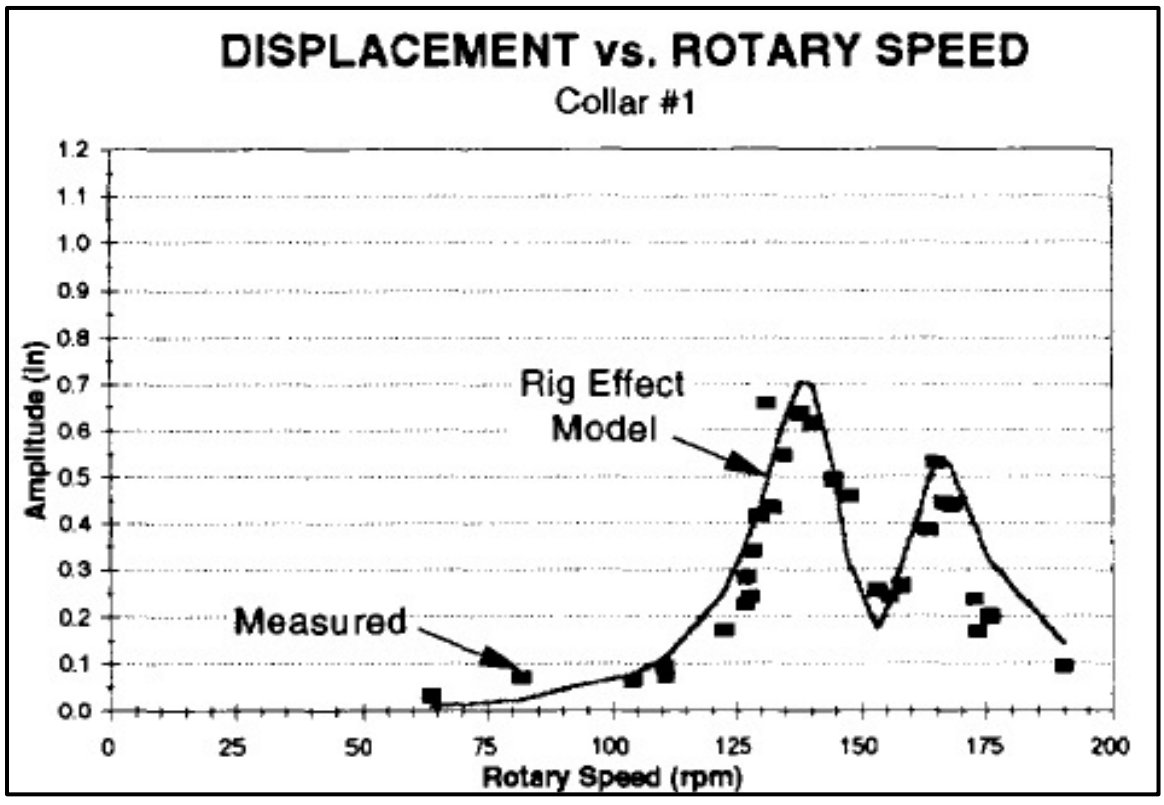

Figure 2.1 Mass imbalance of a drill collar measured as a function of deflection from the borehole center VS rotary speed (Dykstra et al. 1996)

Stick-slip occurs when the static friction of the BHA is higher than dynamic friction due to the transformation of stored drillstring spring energy to inertial energy (Brett 1992). The slip phase starts when the inertial energy is released and leads the drillstring to accelerate to a speed higher than the steady-state rotational speed of the BHA (Brett 1992). If the difference between the static and dynamic friction is high, backward rotation may be observed due to negative torque, which is a main cause for PDC failures (Kriesels et al. 1999). The cause of stick-slip is the non-linear friction interaction between the bit and the rock, which is considered to be self-excited friction-induced torsional vibration (Belokobyl'skii and Prokopov 1982).

2.2. Vibration Modeling

Many attempts were tested to understand the stick/slip motion. One of the first attempts was the pendulum approach, where the drillstring was modeled as a simple torsional pendulum with a single degree-of-freedom at the bit and a fixed end at the rotary table according to the following equation (Halsey et al. 1986; Lin and Wang 1991):

$$I\ddot{\phi} + C\dot{\phi} + F(\dot{\phi}) + K(\phi - \omega t) = 0 \qquad \text{(Eq 2.1)}$$

I= Moment of inertia with respect to the rotary axis (kg.m^2/rad)

$\ddot{\phi}$ = 2nd derivative of angular displacement with respect to time (rad/sec^2)

C= Coefficient of torque due to viscous damping i.e. rotational friction (kg.m^2/rad.sec)

$\dot{\phi}$ = 1st derivative of angular displacement with respect to time (rad/sec)

$F(\dot{\phi})$= The torque due to dry frictional forces (N.m)

K= Torsional stiffness i.e. coefficient of torsion spring – not to be confused with spring constant (N.m/rad)

ϕ = Absolute angular displacement with respect to the earth (rad)

ω = Constant rotary speed (rad/sec)

The following parameters are introduced (Lin and Wang 1991):

$$\omega_0 = \sqrt{\frac{K}{I}}, \omega_0 = \text{undamped natural frequency } \left(\frac{1}{\text{sec}} = \text{Hz}\right) \qquad \text{(Eq 2.2)}$$

$$\zeta = \frac{C}{2\sqrt{KI}}, \zeta = \text{viscous damping ratio (dimensionless)} \qquad \text{(Eq 2.3)}$$

$$f(\dot{\phi}) = \frac{F(\dot{\phi})}{I}, f(\dot{\phi}) = \text{measured in } \left(\frac{\text{rad}}{\text{sec}^2}\right) \quad \text{(Eq 2.4)}$$

The equation can be rearranged to (Lin and Wang 1991):

$$\ddot{\phi} + 2\zeta\omega_0\dot{\phi} + f(\dot{\phi}) + {\omega_0}^2(\phi - \omega t) = 0 \quad \text{(Eq 2.5)}$$

Another mathematical model was proposed by Palmov et al. (1995) where the drillpipe is modeled as one-dimensional in torsion and the BHA is considered as a rigid body. The equation of this model is given as (Palmov et al. 1995):

$$\frac{\partial M}{\partial x} - m - I\frac{\partial^2 \varphi}{\partial t^2} = 0 \quad \text{(Eq 2.6)}$$

M= torque in the drill pipe (N.m)

x= the drillpipe in torsion where 0<x<L (m)

m= moment of external resistance (N)

I= moment of inertia per unit length (kg.m/rad)

$\frac{\partial^2 \varphi}{\partial t^2}$= 2nd derivative of angle of rotation with respect to time (rad/sec^2)

Finite element analysis (FEA) models were considered to solve the complex dynamic behavior of the drillstring. Millheim et al. (1978) were one the first who applied FEA to study the BHA behavior by using the matrix-displacement method. Besaisow et al. (1985) developed a system called Advanced Drillstring Analysis and Measurements System (ADAMS) to detect and analyze the drillstring vibration at the surface using the wave information. An FEA algorithm was developed at Arco Oil & Gas Co by Palsey and Besaisow to study the vibration responses (Besaisow and Payne 1988). This algorithm showed good match with the data obtained by ADAMS (Besaisow and Payne 1988).

Other FEA models were developed by other companies such as a) Drill Strings Dynamics software (DSD) by Shell (Kriesels et al. 1999), b) Forced Frequency Response software (FFR) by DRD Corp (Apostal et al. 1990), c) WHIRL^{TM} software by Halliburton (Chen and Wu 2007), d) Integrated Dynamic Analysis Engineering System (IDEAS) by Smith Technologies (Aslaksen et al. 2006), e) and e) Vybs^{TM} by ExxonMobil (Bailey et al. 2008).

The equation of the motion of a 3D object, with 6 degrees-of-freedom (DOFs) at each node, as shown in Figure 2.2, can be written in a matrix form as follows (Apostal et al. 1990; Aslaksen et al. 2006):

$$[k(t)]x + [C(t)]\dot{x} + [M(t)]\ddot{x} = f(x,t) \qquad \text{(Eq 2.7)}$$

[k]= Spring/elasticity coefficients matrix for specified node (N/m)

x= Displacement vector (m)

[C]= Damping matrix (N.sec/m)

$\dot{x}$= 1st derivative of displacement vector with respect to time i.e. velocity (m/sec)

[M]= Mass matrix (kg)

$\ddot{x}$ = 2nd derivative of displacement vector with respect to time i.e. acceleration (m/sec^2)

$f(x,t)$ = Other external forces vector such as the contact force between cutters and the formation, and the borehole contact with the drill string (N)

Mass

The mass matrix is constructed as a lumped mass matrix that consists of the following:

A) structural mass that contains the mass of drillpipe, drillcollar, bit ... etc.

B) fluid mass inside the drillstring i.e. drilling mud.

C) inertial effects of acceleration of mud outside the drillstring i.e. the mud mass displaced.

D) non-structural mass added by the end-user (Apostal et al. 1990).

Damping

Apostal et al. (1990) broke down the damping matrix into the following four terms:

A) Rayleigh damping that is proportional to both mass [M] and stiffness [k] by the equation:

$$[C_R] = \alpha_R[M] + \beta_R[k] \qquad \text{(Eq 2.8)}$$

Where $\alpha_R \; and \; \beta_R$ are constants of proportionality for mass and stiffness respectively and should satisfy this equation:

$$\zeta = 0.5\left(\frac{\alpha_R}{\omega} + \omega\beta_R\right) \qquad \text{(Eq 2.9)}$$

Where $\zeta \; and \; \omega$ are critical damping ratio and angular frequency (rad/sec).

B) the structural damping is also included in the damping matrix as in the following equation:

$$[C_s] = \frac{2\zeta_s}{\omega}[k] + \frac{2\zeta_c}{\omega}[k_c] \qquad \text{(Eq 2.10)}$$

Where ζ_s and ζ_c are the structural damping ratio from the BHA and contact with the formation, respectively. $[k]$ and $[k_c]$ are the BHA and the contact stiffness matrices, respectively.

C) the third element in the damping matrix is the viscous damping $[C_V]$, which is due to the laminar flow behavior outside the drillstring.

D) the last element is called the additional damping matrix $[C_e]$, which represents the summation of all the finite elements of the BHA.

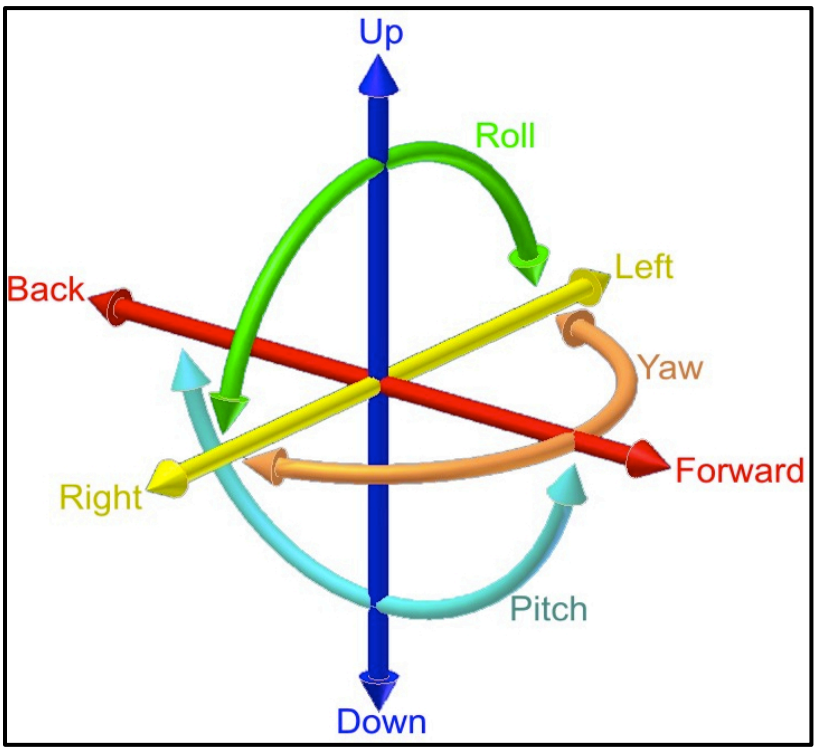

Figure 2.2 The six degrees of freedom (DOFs): Moving up/down, left/right, forward/backward, tilting side/side: roll, left/right: yaw, and forward/backward: pitch (Courtesy of Horia Ionescu: Wikipedia)

2.3. BHA Design

This section will discuss directional drilling assembly designs since they are more complex than the vertical rotary drilling and usually associated with deep drilling. The methods used to drill directional holes are (1) mechanical, (2) hydraulic, and (3) natural (Millheim 1978-1979). Techniques used to drill directional holes are rotary drilling with certain stabilizers arrangements, downhole motor with a bent sub, rotary steerable system (RSS), whipstocks, and jetting drilling. All of these techniques are classified as mechanical methods except the jetting drilling which is considered as a hydraulic method (Millheim 1978-1979). Natural method is related to formation geology such as hardness and dipping associated with a certain BHA design (Millheim 1978-1979). Nowadays, the two most used methods in deep directional drilling are the downhole motor and the RSS.

The principle of the mechanical method depends mainly on directing the resultant side force of the bit toward the desired trajectory (SereneEnergy 2010). The resultant force is the difference between the positive force (build angle) and the negative force (drop angle) (Millheim 1978-1979). Millheim (1978-1979) stated that the positive force depends mainly on stiffness coefficient, inclination, and axial weight, while the negative force depends on the weight suspended below the first point of tangency at a certain trajectory. Factors affecting the bit trajectory include formation hardness, anisotropy, WOB, RPM, bit type, BHA

design, hole diameter and curvature, and flow rate (Walker 1986; SereneEnergy 2010).

Prior to discussing BHA types, some important factors that affect the BHA design will be explained:

1. **Drill collars:** Drill collars provide the WOB needed as well as the rigidity and flexibility to the BHA (Inglis 1987; Short 1993; Azar and Samuel 2007; Aird 2009). The drillstring is designed to keep the drill pipe in tension and the BHA in compression, especially in vertical drilling (API 1998; Kriesels et al. 1999). The point that has zero axial load, called “neutral point”, usually placed in the upper portion of the drill collars to avoid drill pipe buckling (Short 1993; Lyons and Plisga 2005; Aird 2009). Drill collar types include conventional (round diameter), spiral with groove cut, and pony (shorter drill collars) (Inglis 1987; Lyons and Plisga 2005). The spiral collar is used when differential sticking is expected, especially in extended-reach drilling (ERD), by reducing the contact area between the collar and the wellbore (Inglis 1987; Lyons and Plisga 2005; Aird 2009).

   The WOB depends on the density and collar dimensions (Inglis 1987). The stiffness of the drill collar is proportional to the fourth power of the collar diameter given by the moment of inertia equation for a drill collar cross-section area (Millheim 1978-1979; Inglis 1987):

$$\boldsymbol{I = \frac{\pi}{64}(D^4 - d^4)} \qquad \text{(Eq 2.11)}$$

I= Area moment of inertia (in^4)

D= Outside diameter of drill collar (in)

d= Inside diameter of drill collar (in)

Table 2.2 shows the area moment of inertia for different drill collar sizes. It can be seen that stiffness of 10" DC is 16 times the stiffness of 5" DC and 2 times the stiffness of 8" DC (Aird 2009).

Table 2.2 Area moment of inertia for different drill collar sizes (Aird 2009)

OD (in)	ID (in)	I (in^4)
5	2 1/4	29
6 1/4	2 1/4	74
6 1/2	2 1/4	86
6 3/4	2 1/4	101
7	3	114
8	3	197
9	3	318
10	3	487
11	3	715

The required length of the drill collar is given by (Lyons and Plisga 2005; Azar and Samuel 2007):

$$\boldsymbol{L_{DC} = \frac{WOB \times DF}{W_{dc} \times BF \times cos\theta}} \qquad \text{(Eq 2.12)}$$

WOB= Desired weight on bit (lbs.)

DF= Design factor (usually between 1.2-1.3)

$\boldsymbol{W_{dc}}$ = Unit weight of the drill collar in air (lb/ft)

BF= Buoyancy factor = $1 - \frac{\rho_m}{\rho_{dc}}$; $\rho_{dc} = \rho_{steel} = 489.5 \frac{lb}{ft^3} = 65.437 \frac{lb}{gal}$

θ= Angle of inclination

The drill collar section is the most important section to be analyzed in the dynamic analysis since the cross-sectional area is much greater than the drill pipe cross-section area (Dareing 1984). Thus, the drill collar will receive the vibration and amplify it to the drillstring (Dareing 1984).

2. **Heavy-Weight Drill Pipe (HWDP):** HWDPs are used in a transition zone from the drill collar to the drill pipe due to failures occurring in drill pipe section that is just above the drill collar (API 1998). The bending stresses lead to drill pipe fatigue especially in high angle holes (API 1998; Azar and Samuel 2007). Also, the heavy wall pipes are used in lateral sections in deep drilling, instead of drill collars, to decrease torque and drag and differential sticking since heavy weight pipes have less contact area with the wellbore (Inglis 1987; Lyons and Plisga 2005). Generally speaking, increasing the length of the drill collar will have a positive impact on the vibration level by decreasing the natural frequency of the BHA (Dareing 1984). However, coupling drill collars with HWDP is preferable for the following reasons: (1) the cost of handling drill collars is expensive, (2) drill collars will add extra weight that may not be supported by the rig crown block and (3) transition between the drill collar section and the drill pipes by using HWDP is

essential in minimizing fatigue risk of the drillstring (Dareing 1984; API 1998; Azar and Samuel 2007).

3. **Stabilizers:** Stabilizers are short subs with attached blades to the external surface that provide stabilization for the BHA (Inglis 1987; Short 1993). Stabilizers are classified into a) solid type and b) sleeve type (Lyons and Plisga 2005). A solid stabilizer may contain either welded blade or integral blade (Inglis 1987; Lyons and Plisga 2005). Blade configurations can be straight or spiral (Inglis 1987; Lyons and Plisga 2005). Spiral blades have greater surface area contact with the wellbore compared to straight blades, which will help decrease the impact force on the drill collars and reduce the risk of fatigue in the drillstring (Short 1993). The second stabilizer type, sleeve type stabilizer, has a replaceable sleeve attached to the stabilizers body (Inglis 1987; Lyons and Plisga 2005). The advantage of this type, especially when used in hard formations, is that worn blades can be replaced (Inglis 1987; Short 1993). A sleeve stabilizer can be rotating, where it works as solid stabilizer, or non-rotating, where it is used to stiffen and centralize the drill collar in packed-hole BHA (Inglis 1987; Lyons and Plisga 2005). Stabilizer placement plays an important role in hole deviation control, especially with rotary BHA. It should be noted that a stabilizer should be made of non-magnetic material if it is placed close to a survey tool to avoid interference (Inglis 1987).

4. **Reamers:** Reamers are stabilizers with cutting elements that help to ream an under-gauge hole to the desired size and centralize the BHA, especially in hard abrasive formations (Inglis 1987; Short 1993; Lyons and Plisga 2005). Also, reamers help increase the bit efficiency since the bit will work more drilling and less reaming (Lyons and Plisga 2005).
5. **Underreamers:** Underreamers are downhole tools with cutting arms used to enlarge the hole to a bigger size than the bit size (Lyons and Plisga 2005). The arms are initially deactivated (collapsed) when running the drillstring in hole. When the desired depth is reached, increasing mud pressure will activate the cutting arms to start hole enlargement (Lyons and Plisga 2005). Underreamers are classified into: (1) roller cone rock-type, (2) drag-type, and (3) fixed-cutters type as shown in Figure 2.3 and Figure 2.4 (Lyons and Plisga 2005). The roller cone underreamers are used for all types of formations while the drag-type underreamers are used in medium to soft formation (Lyons and Plisga 2005). Underreamers are widely used in Gulf of Mexico (GoM) drilling operations due to the presence of thick salt formations (Compton et al. 2010). Salt sections tend to creep toward the borehole causing problems such as tight hole or stuck pipe (Compton et al. 2010). Underreamers help mitigate salt creep issues by opening the hole to a bigger size (Compton et al. 2010). However, the cutting

forces of underreamers cause additional shock and vibration of the drillstring (Meyer-heye et al. 2011). The movement of underreamers from the borehole center will lead to immediate lateral vibration excitation (Meyer-heye et al. 2011). Placement of underreamers in the BHA is a very important factor in controlling the drillstring vibration.

Best practices for drilling salt sections show that placing an underreamer above the MWD reduces the vibration levels significantly compared with placing it below the MWD (Aburto and D'Ambrosio 2010). Moreover, placing one string stabilizer below the underreamer and one or two stabilizers above it will greatly help centralize the underreamer in the borehole (Aburto and D'Ambrosio 2010). It is also important to run the maximum allowable number and diameter of drill collars above the underreamer to achieve better weight distribution between bit and underreamer (Aburto and D'Ambrosio 2010).

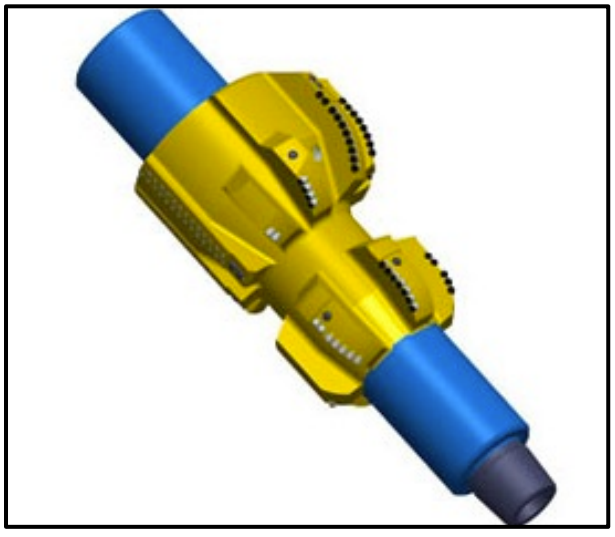

Figure 2.3 Fixed-cutters underreamer type (courtesy of: NOV)

Figure 2.4 Underreamer types (Lyons and Plisga 2005)

6. **Downhole Motors – Positive Displacement Motors (PDM):** A downhole motor with a bent sub is a common way to initiate a kick-off and drill a directional hole. The use of motors in directional drilling is preferred due to less hydraulic power required, availability of different bit and motor sizes, and flexibility of RPM and torque combinations (Short 1993). A PDM consists of a rigid sinusoidal rotor that fits inside an elastomer stator as shown in Figure 2.5 (Short 1993; Lyons and Plisga 2005). Both the rotor and stator have multiple lobes but the stator has always one more lobe than the rotor (Short 1993). As the number of lobes increases, the RPM increases and the torque decreases (Short 1993). Usually, a PDM has between 2 to 7 lobes with an operating speed between 150 to 300 RPM (Short 1993; Lyons and Plisga 2005). PDMs come with a large diameter range that starts from 2 in and can reach up to 9 in (Short 1993). Most roller cone and PDC bits are compatible with PDMs (Short 1993). The drilling mud will flow in the cavities forcing the rotor to rotate within the stator, which will help rotate the bit (Lyons and Plisga 2005). PDMs can be used with most formation rocks and can be operated using the regular rig pumps (Lyons and Plisga 2005). The bent sub is placed above the motor with a length around 2 ft and a deflection angle, in lower portion of the sub, that ranges from 0.5° (for gradual build rate) to 3° (for rapid build rate) (Inglis 1987; Short 1993). The driller adjusts the drillstring orientation to

force the bent sub, motor, and bit toward the desired azimuth while using MWD to measure the orienting of the tool face (Inglis 1987; Short 1993).

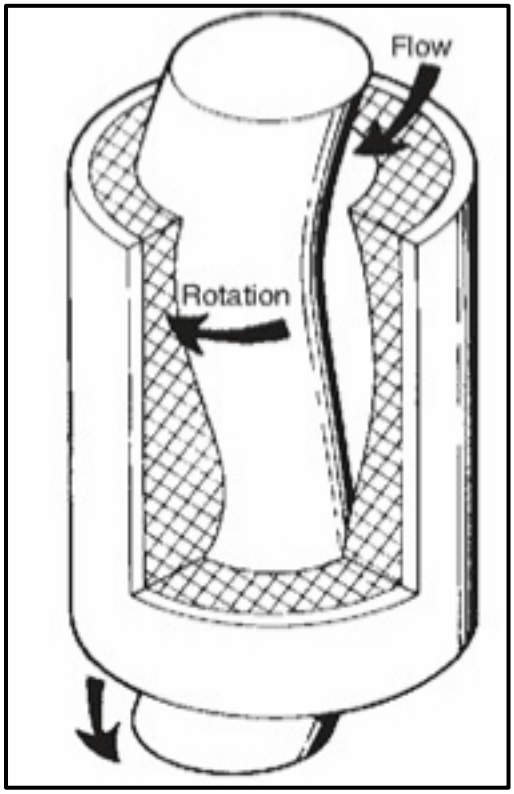

Figure 2.5 A PDM design (Lyons and Plisga 2005)

7. **Downhole Motors – Turbines:** A turbine is used in the same way as the PDM (Short 1993). The turbine has between 25 to 300 stages of rotors and stators with vane angles that rotate the shaft of the motor as it appears in Figure 2.6 (Lyons and Plisga 2005). The turbine is used in holes with a diameter that is 5” or higher because of unavailability of smaller turbine diameters (Short 1993). The use of turbine and a PDC bit is preferable in extremely hard formation since it can improve the

ROP (Lyons and Plisga 2005). However, roller cone bits cannot be used due to the high speed of the motor that will limit the life of the bit (Lyons and Plisga 2005). Also, high efficiency pumps should be used when using a turbine due to the high flow rate needed to compensate for the huge pressure loss across the turbine (Lyons and Plisga 2005).

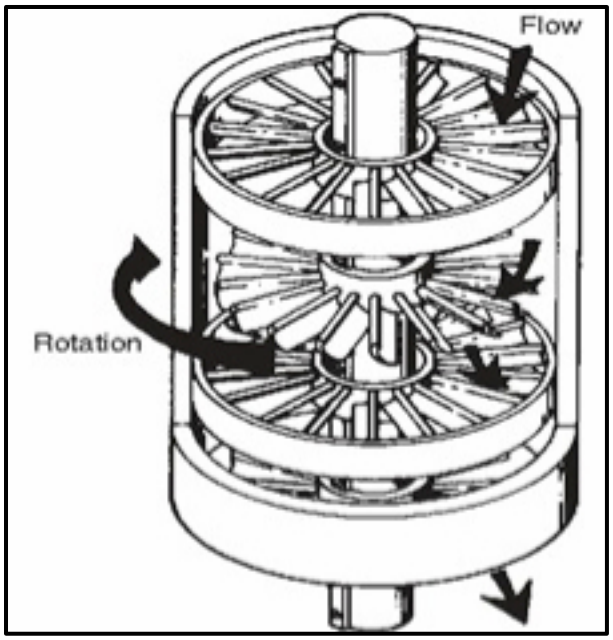

Figure 2.6 A turbine design (Lyons and Plisga 2005)

The BHA is designed to hold, build, or drop angle. The physical principles used for directional drilling are stabilization (hold angle), fulcrum (build angle), and pendulum (drop angle) approaches as shown in Figure 2.7 (SereneEnergy 2010).

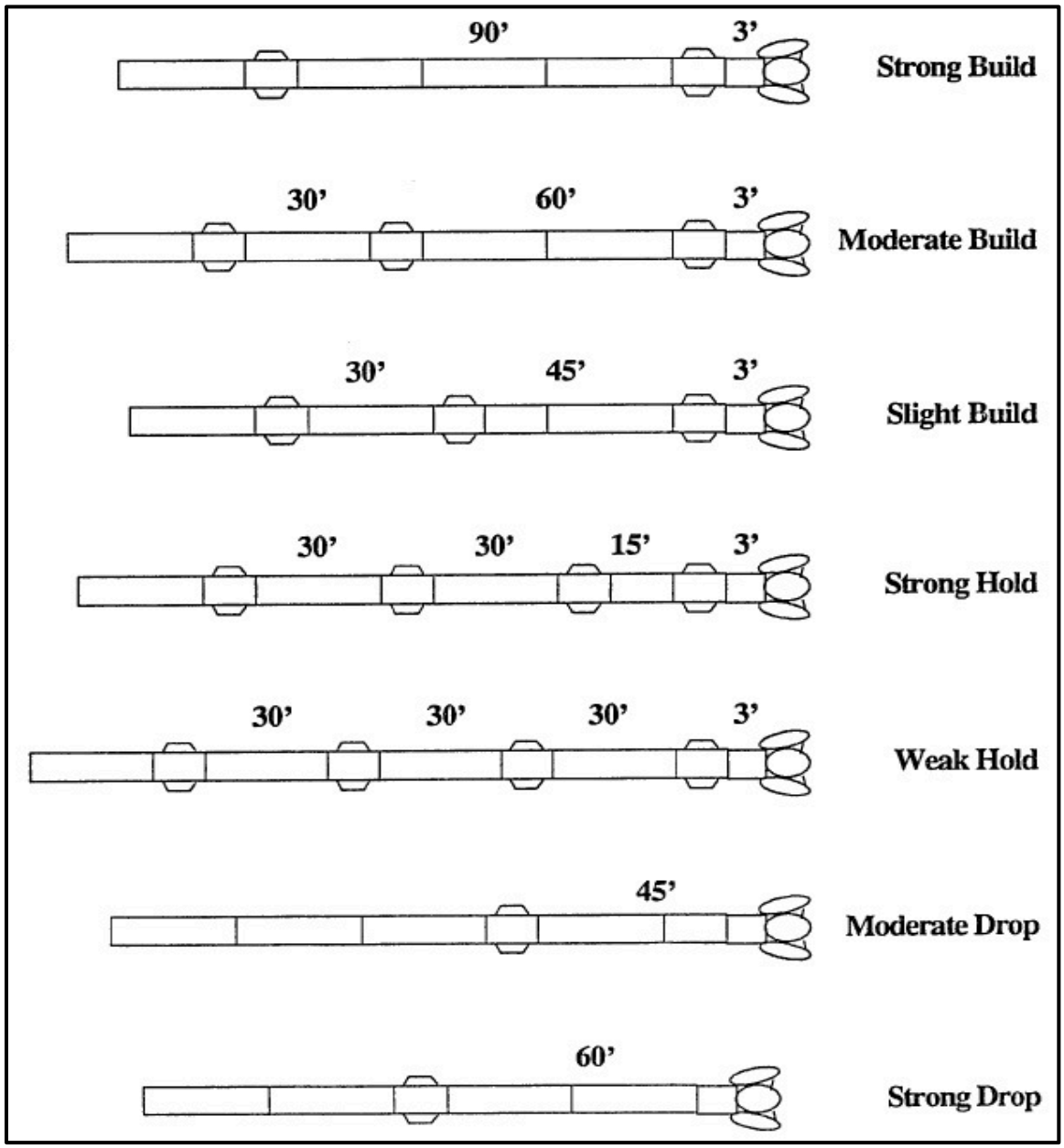

Figure 2.7 Common BHA designs and the expected responses (Walker 1986; Payne 1992)

2.3.1. Building Assembly

One of the most important factors affecting the building assembly is the stabilizer(s) placement (Millheim 1978-1979; Walker 1986; SereneEnergy 2010). A stabilizer that is very close to the bit (5-10 ft), usually called near-bit stabilizer, will act as a fulcrum or pivot with long lever, which will increase the upward positive force (building angle) when followed by 40-120 ft of drill collars (Millheim 1978-1979; Walker 1986; SereneEnergy 2010). Another stabilizer is usually placed above the drill collars so that the drill collars will bend, due to WOB and their own weight, and push the bit away from the hole axis (Walker 1986; SereneEnergy 2010). The two stabilizers are usually replaced by roller reamers in hard abrasive formations to keep the hole in gauge since the bit wear is faster (Inglis 1987).

The increase in the distance between the near-bit stabilizer and the first string stabilizer will increase the rate of inclination build (Walker 1986; SereneEnergy 2010). Increasing the WOB will increase the build rate but the effect will decrease when the inclination increases (Millheim 1978-1979; SereneEnergy 2010). Decreasing the drill collars diameter will increase the build rate (Short 1993; SereneEnergy 2010). Low rotary speed (70-100 ft) is preferable to build angle since high RPM will tend to straighten the drill collars, which will reduce the build rate (SereneEnergy 2010).

2.3.2. Dropping Assembly

The slick assembly (or the pendulum assembly) is used to drop the inclination by placing a single stabilizer 30-60 ft from the bit (Millheim 1978-1979; Walker 1986; SereneEnergy 2010). The contact between the stabilizer and the hole will bring the bit toward the vertical direction since the drill collars below the stabilizer will act as a pendulum because of their weight (Walker 1986; SereneEnergy 2010). It is important to reduce the drill collars contact with the low side of the hole since the contact will reduce the negative side forces that brings the BHA toward the vertical axis (SereneEnergy 2010). It is good to begin with a low WOB to initiate the dropping section, and then increase the WOB so that the ROP increases (SereneEnergy 2010). Generally speaking, high RPM helps straightening the pendulum portion (that starts from the bit to the stabilizer) and avoiding the pendulum from laying on the low side of the hole (SereneEnergy 2010). High inclination hole will increase the dropping tendency of a pendulum assembly (Callas and Callas 1980; SereneEnergy 2010). The pendulum assembly will not be a good choice to drop the inclination in a hard formation since the side forces are not enough to cut the rock (Millheim 1978-1979; SereneEnergy 2010). Gradual inclination build to the desired trajectory is preferable over an inclination drop (Millheim 1978-1979).

2.3.3. Holding Assembly

Packed-hole assembly or multi-stabilizer assembly is used to hold angle in directional drilling applications (Millheim 1978-1979; Walker 1986). The force that

keep the drillstring centered in the hole and keeps the inclination constant depends greatly on the rigidity and stiffness of the BHA (Short 1993). The stiff, rigid BHA will force the drillstring to follow the same previous hole direction (Short 1993). Holding the angle in a very soft formation is an easy task by using low WOB (Millheim 1978-1979). Millheim (1978-1979) suggested using 6-7 in drill collar for holes less than 12 ¼ in and 7-8 in collar for holes larger than 12 ¼ in. Maintaining the inclination in a medium-soft formation is difficult since the bit still has side forces while drilling, preventing the BHA from holding the angle (Millheim 1978-1979; Inglis 1987). To help holding the inclination, three stabilizers should be placed closed to each other and pony collars are suggested (Millheim 1978-1979; Inglis 1987).

3. CASE STUDY: MANIFA FIELD

The Manifa field, the fifth largest oil field in the world measuring 28 miles in length and 11 miles in width, was discovered in 1957 with 11 billion barrels of heavy crude oil reserves (Jafee and Elass 2007; Bartko et al. 2009; SaudiAramco 2010). It is located on the Arabian Gulf offshore around 124 miles northwest of Dhahran, Saudi Arabia (Saudi Aramco Headquarter) as shown in Figure 3.1 (SaudiAramco 2010). Saudi Aramco started the Manifa mega project in 2006 to produce a target of 900,000 bpd (Barrels Per Day) of Arabian heavy crude oil, 90 million scfd (Standard Cubic Feet per Day) of associated gas, and 65,000 bpd of condensate by 2014 (SaudiAramco 2010).

The location of the Manifa field in unusually shallow environmentally sensitive seawater, which can reach up to 131 ft in depth, led to the decision to build 27 man-made islands designed to drill the shallow water wells (Bartko et al. 2009; SaudiAramco 2010). These artificial islands have a dimension of 1,115 ft × 853 ft for each island and are connected by 24 miles of causeways as shown in Figure 3.2 (SaudiAramco 2010). An additional 13 offshore platforms are used to drill deep water wells (SaudiAramco 2010). The targeted oil bearing reservoirs are Lower Ratawi and Manifa, which are limestone with dolomite intervals (Bartko et al. 2009). Figure 3.3 shows a schematic of a Manifa PWI (Power Water Injection) well that will be studied in this report.

Figure 3.1 Manifa oil field location on the Arabian Gulf (source: Saudi Aramco)

Figure 3.2 A drilling island in the Manifa project

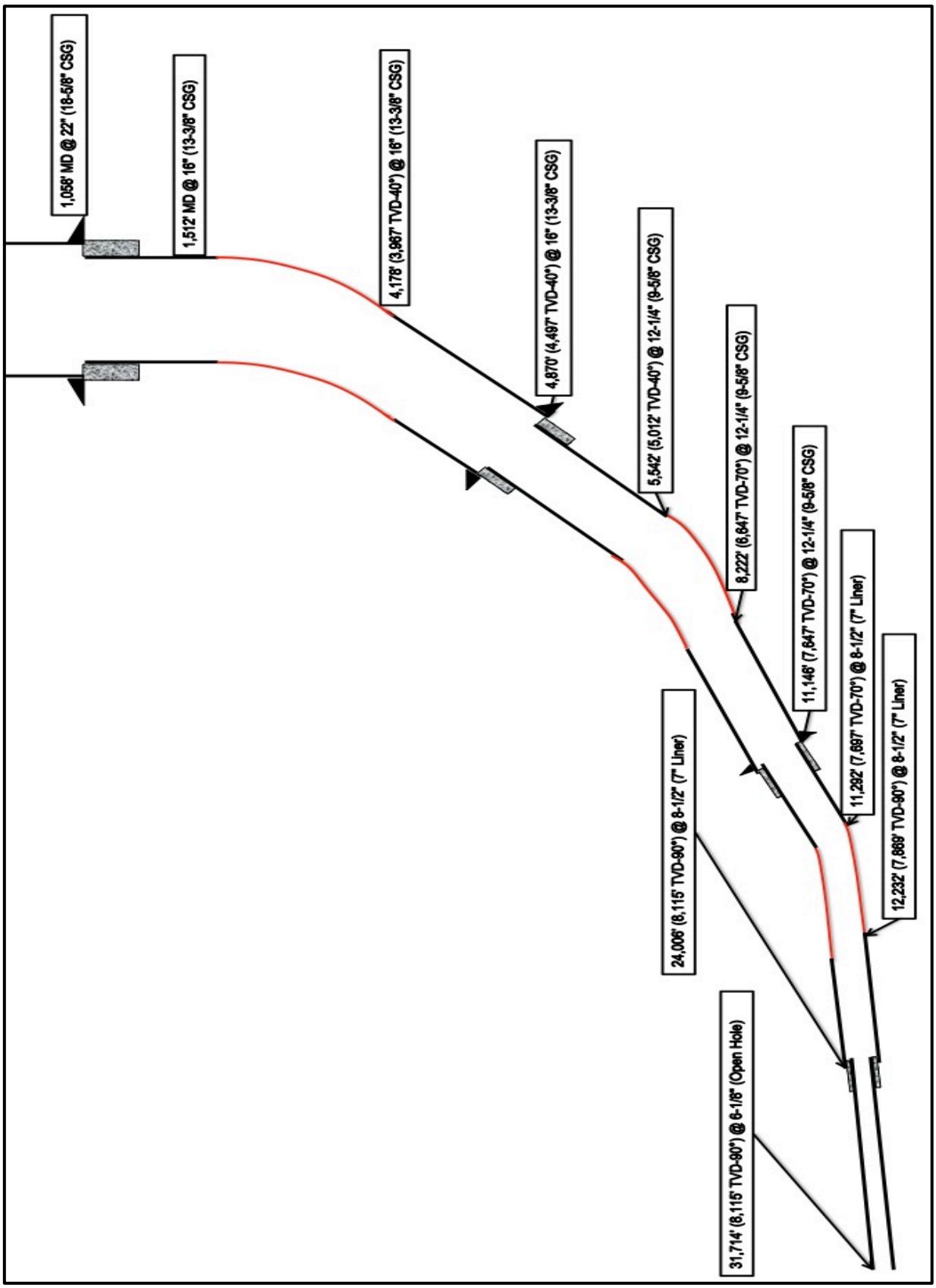

Figure 3.3 A schematic for a Manifa PWI well

3.1. Manifa 12-1/4" Hole (PWI)

This section was drilled from 4,870' MD (4,497' TVD) to 9-5/8" casing point at 11,146' MD (7,847' TVD – 40° inclination). The purpose of casing is to shut off lost circulation intervals and cover unstable shale. Before starting the dynamic analysis of the BHA design, basic static design will be discussed. First, WOB is specified in addition to the mud density (pound per gallon – ppg). These values are determined based on the reservoir fluid properties, formation, and other risk associated with the field like torque and drag and stuck pipe risk. The design started by determining the drill collar length required to apply certain weight on bit. Usually, more than one size of drill collars are used i.e. tapered drill collars design. To calculate the WOB resulting from a tapered design, (Eq 2.12) is modified as follow:

$$\boldsymbol{WOB} = \frac{(\boldsymbol{L_{dc1}W_{dc1}} + \boldsymbol{L_{dc2}W_{dc2}} + \boldsymbol{L_{dc3}W_{dc3}})\times \boldsymbol{BF}\times \boldsymbol{cos\theta}}{\boldsymbol{DF}} \qquad \text{(Eq 3.1)}$$

WOB= Desired weight on bit (lbs.)

DF= Design factor (usually between 1.2-1.3)

$\boldsymbol{W_{dc}}$ = Unit weight of the drill collar in air (lb/ft)

$\boldsymbol{L_{dc}}$ = Length of the drill collar (ft)

BF= Buoyancy factor = $1 - \frac{\rho_m}{\rho_{dc}}$; $\rho_{dc} = \rho_{steel} = 489.5\frac{lb}{ft^3} = 65.437\frac{lb}{gal}$

θ= Angle of inclination

As stated before, the drill collars are designed to be in compression mode while the drill pipe (and the heavy weight drill pipe HWDP) are designed to

be in tension. The point of zero axial load (called neutral point) is usually located around 80-85 % (denoted by 20-15 % safety factor) of the total drill collar(s) length. For deep, small-hole, high-inclination drilling operations, drill pipe is commonly used in compression without the use of drill collars (Dawson and Paslay 1984). Studies showed that drill pipe can tolerate high compression loads without failures because it is supported by the low side of the hole (Dawson and Paslay 1984). This would be beneficial in ERD wells since removing the drill collars will reduce the torque and drag (Dawson and Paslay 1984).

Then, the maximum length of drill pipe is calculated based on the margin of overpull (MOP) and the mud density in the hole (ppg). If the maximum length is shorter than the required length, then a stronger drill pipe is required. Tapered design of drill pipe is also common in field operations. All drill pipe calculations in this thesis assume API premium class inspection (used pipe). The length of the maximum drill pipe is given by the equation:

$$\frac{P_{t1}\times 0.9 - MOP}{W_{dp1}\times K_b} - \frac{W_c\times L_c}{W_{dp1}} = L_{dp1} \qquad \text{(Eq 3.2)}$$

P_t = theoretical tension load for a drill pipe from API table, lb.,

0.9 = a constant relating proportional limit to yield strength.

(Eq 3.2) is used if only one drill pipe size and grade is used. It would also be also used to calculate the maximum length of the weaker drill pipe if a tapered drill string design is used. The length of the stronger drill pipe is given by:

$$\frac{P_{t2}\times 0.9 - MOP}{W_{dp2}\times K_b} - \frac{(W_c\times L_c) + (W_{dp1}\times L_{dp1})}{W_{dp2}} = L_{dp2} \qquad \text{(Eq 3.3)}$$

The drill pipe with the lowest strength is placed just above the drill collar and then the stronger one.

The static design and well properties are shown in Table 3.1. The left section of the table shows the drill collar joints and the weight that is applied by the downhole tools, drill collars, and HWDP. The applied weight formula for the BHA is based on (Eq 3.1). It can be noticed that the applied weight is less than the required WOB (14,458 lb < 25,000). This is not surprising since the inclination is high i.e. 70°. Thus, part of the drill pipe section will be put in compression. The right section of the table shows the drill pipe properties ensuring that the maximum allowable drill pipe length is greater than the required drill pipe length. The details of the BHA segments are shown in Table 3.2. This data is required as input for the software tool so that it can show the analysis.

The critical speeds for the 3 BHA configurations tabulated in Table 3.2, Table 3.3, and Table 3.4 are shown in Figure 3.4, Figure 3.5, and Figure 3.6, respectively. The modified parameter from the original design (BHA#1) has been shaded in the modified BHA tables to track changes easier. All the dynamic analysis in this report was done using Vibrascope™, which was developed by NOV.

Table 3.1 Static BHA analysis for Manifa 12-1/4" hole (PWI well)

Well Properties			
Required WOB		25,000	lb
Mud Weight		10.026	ppg
BF		0.847	
Hole Inclination		70	°
MOP		30,000	lb

Drill Collar Design			
1	OD	8.250	in
	ID	2.875	in
	W_{dc}	160	lb/ft
	# of joints	3	
	L_{dc}	108	ft
2	OD	0	in
	ID	0	in
	W_{dc}	0	lb/ft
	# of joints	0	
	L_{dc}	0	ft
3	OD	0	in
	ID	0	in
	W_{dc}	0	lb/ft
	# of joints	0	
	L_{dc}	0	ft
SF		20%	
Applied Weight (motors+DC+HWDP)		14,458	lb

Drill Pipe Design			
Bottom Section	OD	5.500	in
	ID	4.778	in
	W_{dp}	21.9	lb/ft
	P_t (E75)	311,535	lb
	L_{dp}	13,142	ft
Top Section	OD	0	in
	ID	0	in
	W_{dp}	0	lb/ft
	P_t	0	lb
	L_{dp}	0	ft
BHA Submerged Load P		241,587	lb

Table 3.2 Dynamic data input for Manifa 12-1/4" hole BHA#1 (PWI well)

BHA#1: Manifa (12.25" hole section)						
String Geometry & Material						
BHA	Length (ft)	Cum Length (ft)	OD (in)	ID (in)	Weight (lb)	Material
12 1/4" PDC	1.10	1.1	12.250		500	Steel
Xceed 900 stabilizer	28.30	29.4	9.000	6.750	4,500	Steel
Downhole Filter Sub	3.75	33.2	8.250	3.000	200	Steel
PowerPak mud motor	31.50	64.7	9.625	7.850	4,000	Steel
8-1/4" NMDC	14.30	79.0	8.250	4.250	2,288	Steel
LSS	1.30	80.3	8.250	5.900	200	Steel
PowerPulse 825	24.74	105.0	8.250	4.250	3,000	Steel
USS	1.54	106.5	8.250	2.875	200	Steel
8-1/4" NMDC	30.41	136.9	8.250	3.000	4,866	Steel
Downhole Filter Sub	3.80	140.7	8.250	3.000	200	Steel
PBL - SUB	14.79	155.5	8.250	2.500	864	Steel
1 X 8-1/4" DC	30.26	185.8	8.500	2.875	4,842	Steel
Hydraulic Mech Jar	33.13	218.9	8.000	2.750	2,200	Steel
1 X 8-1/4" DC	31.26	250.2	8.500	2.875	5,002	Steel
X - O	1.80	252.0	10.000	3.000	450	Steel
15 X 5-1/2" HWDP	461.70	713.7	6.625	3.375	26,594	Steel
332 X 5-1/2" DP	10,292.00	11,005.7	5.500	4.778	225,395	Steel
				Total Air Weight (lb)	**285,300**	
Borehole Geometry						
12.25"						
3D Well path						
Inclination	70°		Azimuth	26		
WOB (lb)						
25,000						
Mud Weight (ppg)						
10.026						

Table 3.3 Dynamic data input for Manifa 12-1/4" hole BHA#2 (PWI well)

BHA#2: Manifa (12.25" hole section)						
String Geometry & Material						
BHA	Length (ft)	Cum Length (ft)	OD (in)	ID (in)	Weight (lb)	Material
12 1/4" PDC	1.10	1.1	12.250		500	Steel
Xceed 900 stabilizer	28.30	29.4	9.000	6.750	4,500	Steel
Downhole Filter Sub	3.75	33.2	8.250	3.000	200	Steel
PowerPak mud motor	31.50	64.7	9.625	7.850	4,000	Steel
8-1/4" NMDC	14.30	79.0	8.250	4.250	2,288	Steel
LSS	1.30	80.3	8.250	5.900	200	Steel
PowerPulse 825	24.74	105.0	8.250	4.250	3,000	Steel
USS	1.54	106.5	8.250	2.875	200	Steel
8-1/4" NMDC	30.41	136.9	8.250	3.000	4,866	Steel
Downhole Filter Sub	3.80	140.7	8.250	3.000	200	Steel
PBL - SUB	14.79	155.5	8.250	2.500	864	Steel
1 X 8-1/4" DC	30.26	185.8	8.500	2.875	4,842	Steel
Hydraulic Mech Jar	33.13	218.9	8.000	2.750	2,200	Steel
2 X 8-1/4" DC	62.52	281.4	8.500	2.875	10,003	Steel
X - O	1.80	283.2	10.000	3.000	450	Steel
14 X 5-1/2" HWDP	430.92	714.2	6.625	3.375	24,821	Steel
332 X 5-1/2" DP	10,292.00	11,006.2	5.500	4.778	225,395	Steel
				Total Air Weight (lb)	**288,528**	
Borehole Geometry						
12.25"						
3D Well path						
Inclination	70°		Azimuth	26		
WOB (lb)						
25,000						
Mud Weight (ppg)						
10.026						

Table 3.4 Dynamic data input for Manifa 12-1/4" hole BHA#3 (PWI well)

BHA#3: Manifa (12.25" hole section)						
String Geometry & Material						
BHA	Length (ft)	Cum Length (ft)	OD (in)	ID (in)	Weight (lb)	Material
12 1/4" PDC	1.10	1.1	12.250		500	Steel
Xceed 900 stabilizer	28.30	29.4	9.000	6.750	4,500	Steel
Downhole Filter Sub	3.75	33.2	8.250	3.000	200	Steel
PowerPak mud motor	31.50	64.7	9.625	7.850	4,000	Steel
8-1/4" NMDC	14.30	79.0	8.250	4.250	2,288	Steel
LSS	1.30	80.3	8.250	5.900	200	Steel
PowerPulse 825	24.74	105.0	8.250	4.250	3,000	Steel
USS	1.54	106.5	8.250	2.875	200	Steel
8-1/4" NMDC	30.41	136.9	8.250	3.000	4,866	Steel
Downhole Filter Sub	3.80	140.7	8.250	3.000	200	Steel
PBL - SUB	14.79	155.5	8.250	2.500	864	Steel
2 X 8-1/4" DC	60.52	216.1	8.500	2.875	9,683	Steel
Hydraulic Mech Jar	33.13	249.2	8.000	2.750	2,200	Steel
3 X 8-1/4" DC	93.78	343.0	8.500	2.875	15,005	Steel
X - O	1.80	344.8	10.000	3.000	450	Steel
12 X 5-1/2" HWDP	369.36	714.1	6.625	3.375	21,275	Steel
332 X 5-1/2" DP	10,292.00	11,006.1	5.500	4.778	225,395	Steel
				Total Air Weight (lb)	**294,826**	
Borehole Geometry						
12.25"						
3D Well path						
Inclination	70°		Azimuth	26		
WOB (lb)						
25,000						
Mud Weight (ppg)						
10.026						

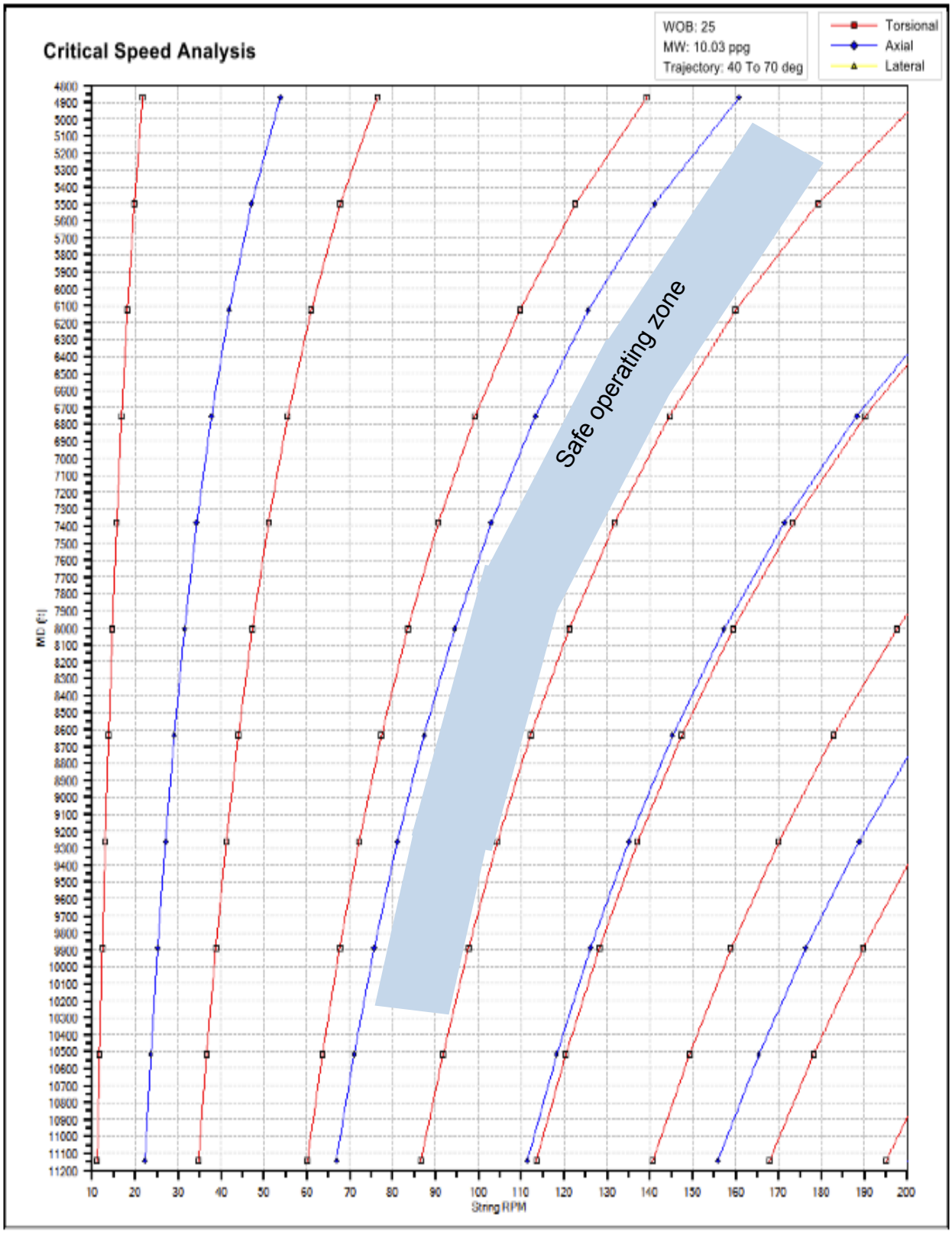

Figure 3.4 Critical speeds for Manifa 12-1/4” hole BHA#1

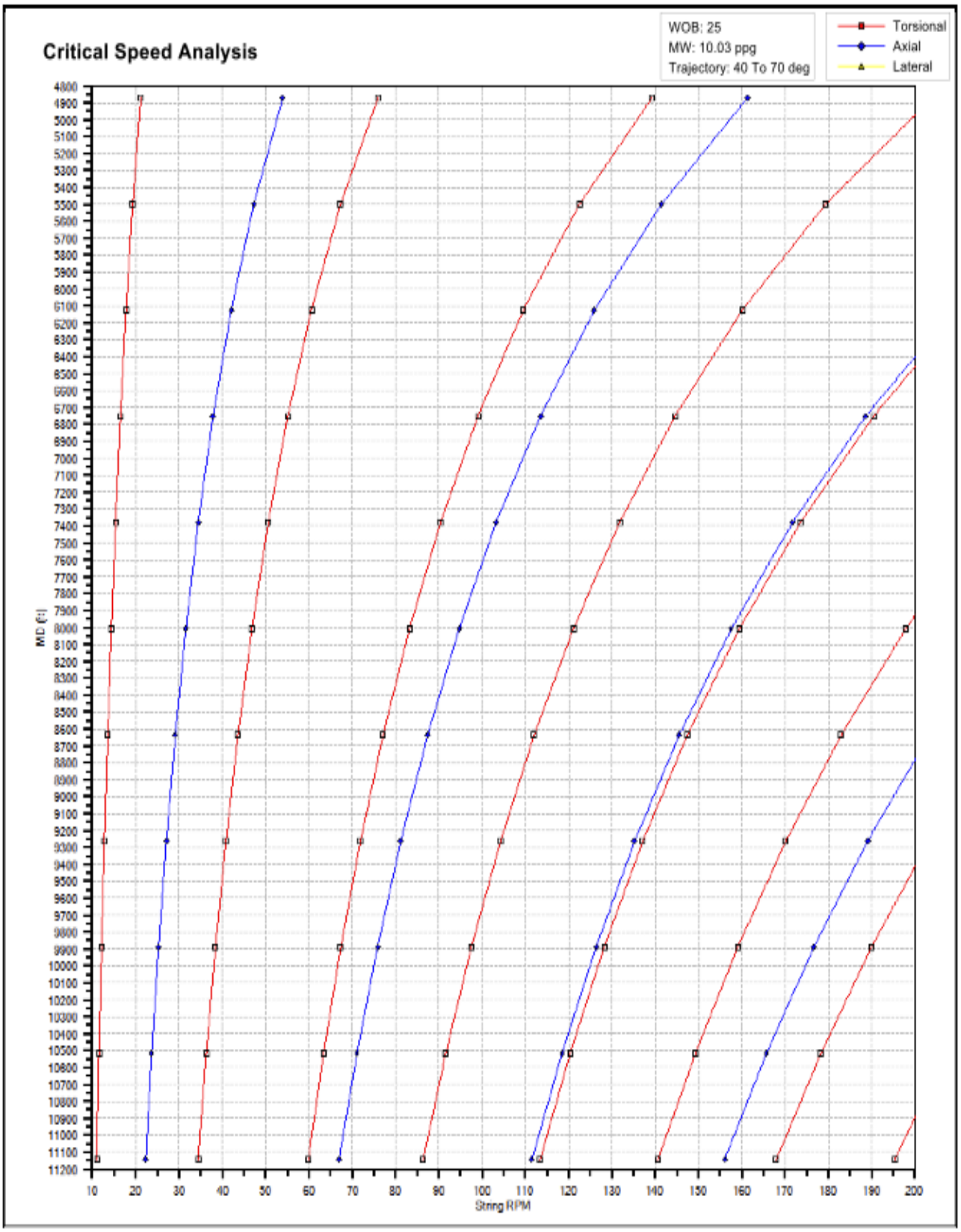

Figure 3.5 Critical speeds for Manifa 12-1/4” hole BHA#2

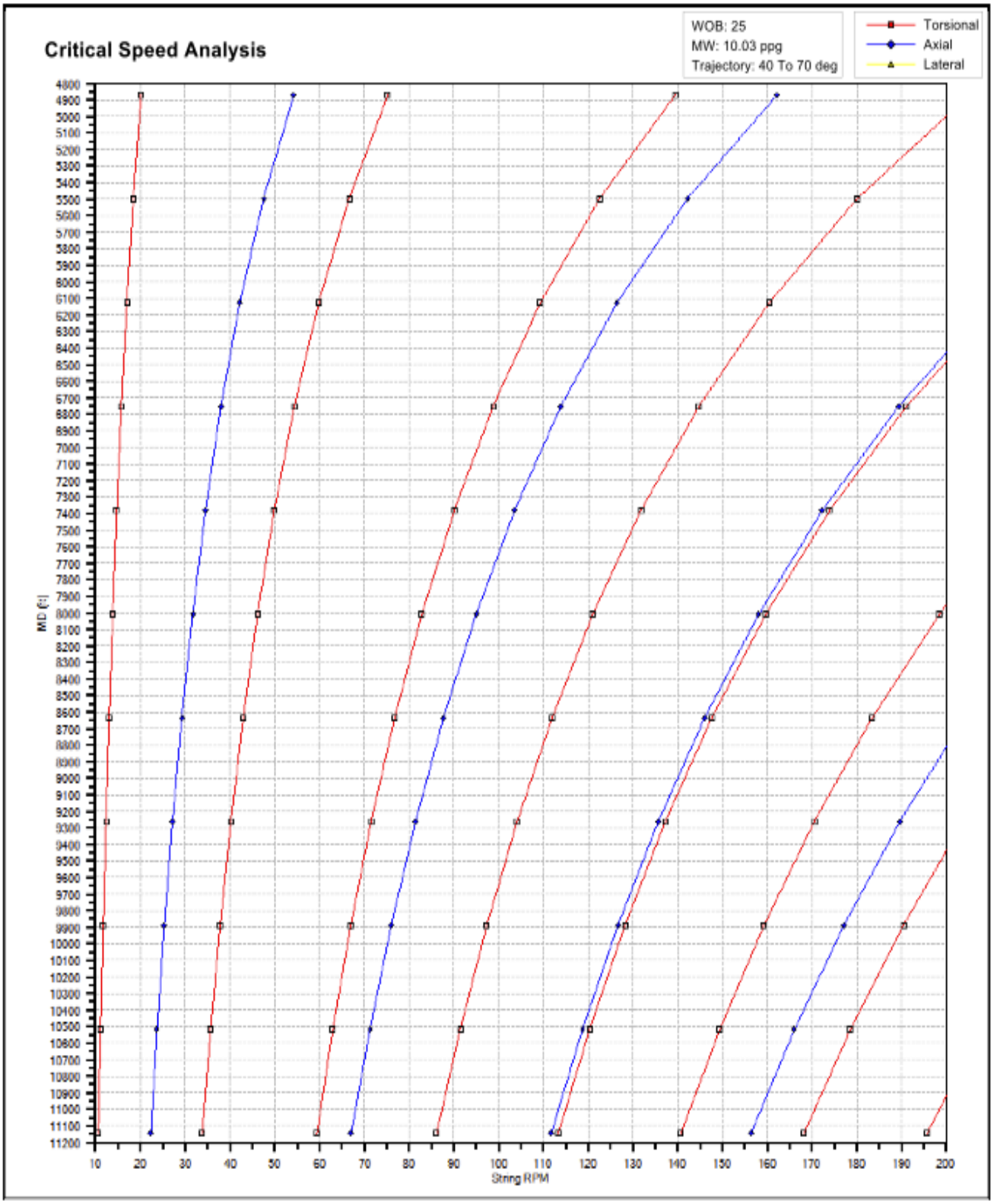

Figure 3.6 Critical speeds for Manifa 12-1/4” hole BHA#3

BHA#1 configuration shows good critical speeds range as shown in Figure 3.4. It is believed that the presence of higher OD drill collar plus the HWDP helps in dampening the vibration at many depth ranges. The high area moment of inertia (also called second moment of inertia) of drill collars increases the stiffness of the BHA and, consequently, minimize the deflection. This will increase the safe operating speed of the drillstring. Dykstra et al. (1996) suggested to rotate the drill string at a speed that is higher than the critical speed if resonance occurred at lower speeds (60 RPM), especially when multiple resonant speeds are present. On the other hand, if resonance occurred at higher speeds (120 RPM), it is a good practice to stay lower than this speed. Going above a high critical speed may result in changing the bit motion from the normal forward motion to the destructive backward motion (Dykstra et al. 1996).

The BHA was redesigned twice to see the effect of drill collars in terms of critical speed change. Two 8-1/2” drill collar joints were run in BHA#2 just above the mechanical jar (instead of 1 drill collar as in BHA#1). The number of HWDP joints was reduced to 14 (instead of 15). For BHA#3, two 8-1/2” drill collar joints were placed below the mechanical jar and three 8-1/2” drill collar joints were placed above the mechanical jar. HWDP joints were reduced to 12 joints. This redesign aimed to stiffen the BHA to reduce the vibration. However, the critical speed ranges for BHA#2 and BHA#3, shown in Figure 3.5 and Figure 3.6, have not change that much from the speed range for BHA#1 as in Figure 3.4. The big

change in drill collar joints has not lead to any change in critical speed range. Also, it can be noticed that lateral vibration is not present in any of the BHAs.

3.2. Manifa 8-1/2" Hole (PWI)

This hole section was drilled from 11,146' MD (7,847' TVD) to the 7" liner point at 24,000' MD (8,115' TVD – 90° inclination). BHA#1 properties are shown in Table 3.5 and Table 3.6. No drill collars were used in BHA#1 except 2 non-magnetic collars used to isolate the MWD. BHA#2 configuration is shown in Table 3.7. Critical speeds for the 2 BHA configurations are shown in Figure 3.7 and Figure 3.8, respectively.

Table 3.5 Static BHA analysis for Manifa 8-1/2" hole (PWI well)

Well Properties							
Required WOB				25,000	lb		
Mud Weight				10.026	ppg		
BF				0.847			
Hole Inclination				90	°		
MOP				30,000	lb		
Drill Collar Design				**Drill Pipe Design**			
1	OD	0	in	Bottom Section	OD	5.000	in
	ID	0	in		ID	4.276	in
	W_{dc}	0	lb/ft		W_{dp}	19.5	lb/ft
	# of joints	0			P_t(S135)	560,764	lb
	L_{dc}	0	ft		L_{dp}	27,840	ft
2	OD	0	in	Top Section	OD	0	in
	ID	0	in		ID	0	in
	W_{dc}	0	lb/ft		W_{dp}	0	lb/ft
	# of joints	0			P_t	0	lb
	L_{dc}	0	ft		L_{dp}	0	ft
SF		20%		BHA Submerged Load P		407,122	lb
Weight Applied by the BHA		0	lb				

Table 3.6 Dynamic data input for Manifa 8-1/2" hole BHA#1 (PWI well)

BHA#1: Manifa (8.5" hole section)						
String Geometry & Material						
BHA	Length (ft)	Cum Length (ft)	OD (in)	ID (in)	Weight (lb)	Material
8-1/2"PDC BIT	0.83	0.8	12.250		500	Steel
XCEED 675 motor	25.10	25.9	6.750	5.160	2,620	Steel
NMSS	1.15	27.1	6.750	3.250	200	Steel
TELESCOPE 675	25.13	52.2	6.750	5.109	2,085	Steel
NMSS	1.60	53.8	6.750	3.250	200	Steel
6-3/4" NMDC	29.55	83.4	6.750	2.870	2,955	Steel
FILTER SUB	8.00	91.4	6.750	3.460	200	Steel
1 X 5" HWDP	30.94	122.3	6.500	2.875	1,525	Steel
JAR	34.35	156.7	6.500	2.875	1,400	Steel
4 X 5"HWDP	122.80	279.5	6.500	2.875	6,054	Steel
766 X 5"DP	23,746.00	24,025.5	5.000	4.276	463,047	Steel
				Total Air Weight (lb)	**480,786**	
Borehole Geometry						
8.5"						
3D Well path						
Inclination	89°		Azimuth	26		
WOB (lb)						
25,000						
Mud Weight (ppg)						
10.026						

Table 3.7 Dynamic data input for Manifa 8-1/2" hole BHA#2 (PWI well)

BHA#2: Manifa (8.5" hole section)						
String Geometry & Material						
BHA	Length (ft)	Cum Length (ft)	OD (in)	ID (in)	Weight (lb)	Material
8-1/2"PDC BIT	0.83	0.8	12.250		500	Steel
XCEED 675 motor	25.10	25.9	6.750	5.160	2,620	Steel
NMSS	1.15	27.1	6.750	3.250	200	Steel
TELESCOPE 675	25.13	52.2	6.750	5.109	2,085	Steel
NMSS	1.60	53.8	6.750	3.250	200	Steel
6-3/4" NMDC	29.55	83.4	6.750	2.870	2,955	Steel
FILTER SUB	8.00	91.4	6.750	3.460	200	Steel
2 X 6-1/2" DC	62.00	153.4	6.500	2.813	5,642	Steel
1 X 5" HWDP	30.94	184.3	6.500	2.875	1,525	Steel
JAR	34.35	218.7	6.500	2.875	1,400	Steel
4 X 5"HWDP	122.80	341.5	6.500	2.875	6,054	Steel
764 X 5"DP	23,684.00	24,025.5	5.000	4.276	461,838	Steel
				Total Air Weight (lb)	**485,219**	
Borehole Geometry						
8.5"						
3D Well path						
Inclination	89°		Azimuth	26		
WOB (lb)						
25,000						
Mud Weight (ppg)						
10.026						

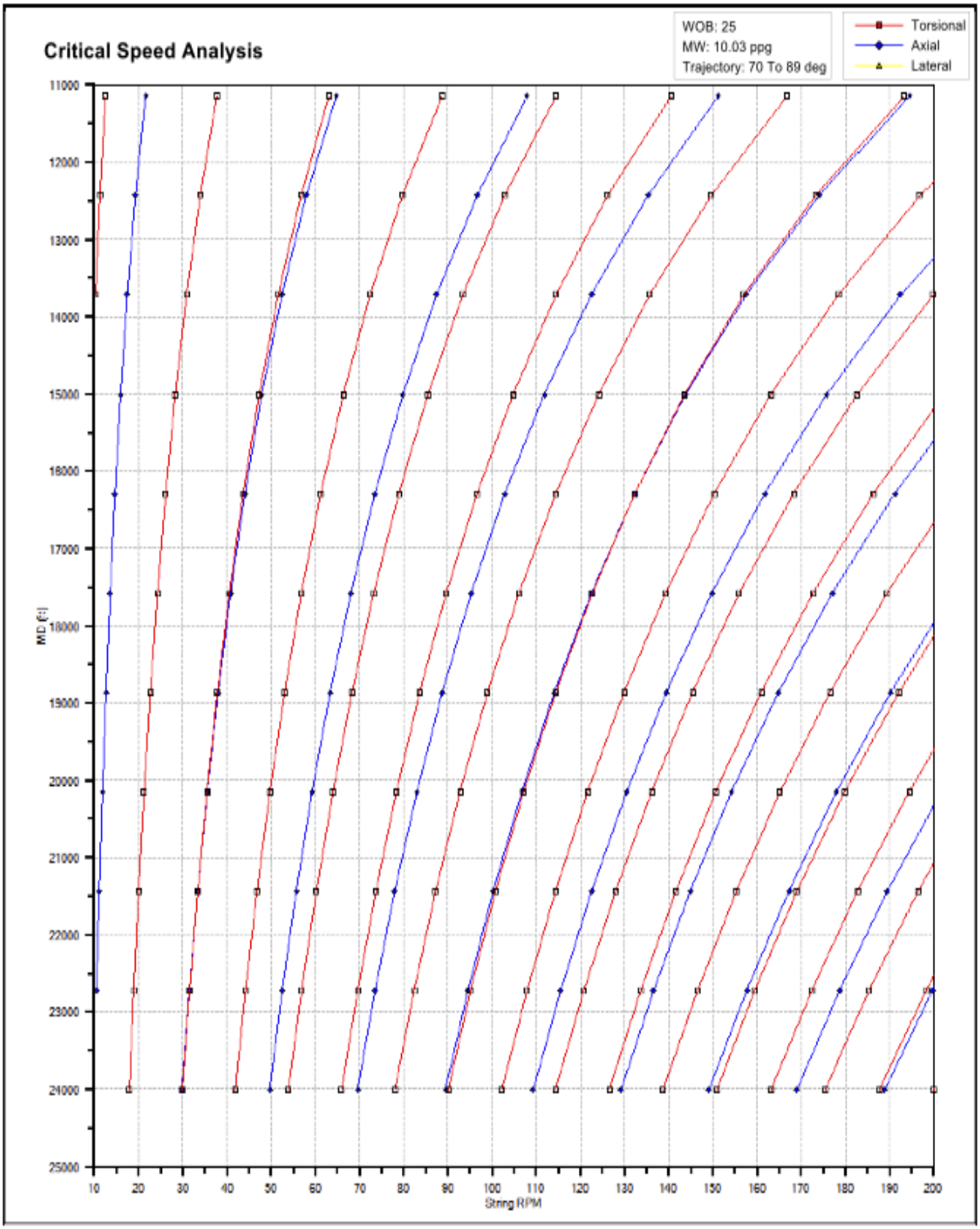

Figure 3.7 Critical speeds for Manifa 8-1/2” hole BHA#1

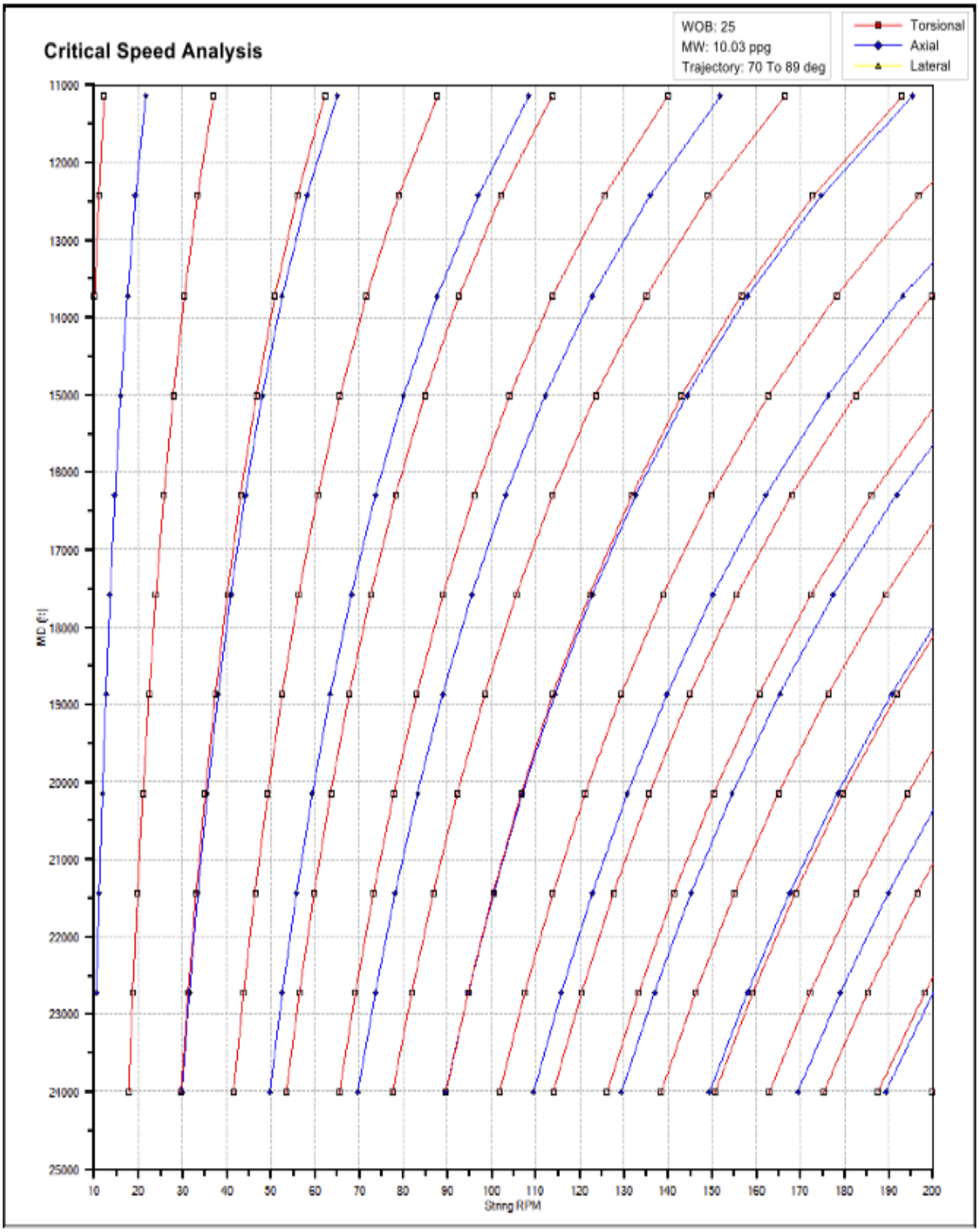

Figure 3.8 Critical speeds for Manifa 8-1/2” hole BHA#2

BHA#1 configuration shows a short safe operating speed range as in Figure 3.7. The range is going in a curvy shape that would require changing the RPM as going down. The increase length of the drillstring in addition to relatively small hole size leads to decreasing the operating speed. It is believed that the absence of drill collars in the BHA may lead to this problem. Thus, 2 joints of 6-1/2” drill collars have been introduced in the redesigned BHA (BHA#2). The addition of drill collars will stiffen the drill string and thus may reduce the vibration. However, as in the previous hole section, the change in the BHA configuration did not result in a change in the operating speed range as in Figure 3.8. It seems that the length of the drill string will affect the speed range much more than changing BHA parameters, especially for long sections (13,000 ft) such as this one. Lateral vibration is not present in both figures.

3.3. Manifa 6-1/8” Hole (PWI)

This hole section was drilled from 24,000’ MD (8,115’ TVD – 90° inclination) to the Lower Ratawi reservoir TD (target depth) at 31,700’ MD (8,115’ TVD – 90° inclination). BHA#1 properties are shown in Table 3.8 and Table 3.9. BHA#2 configuration is shown in Table 3.10. Critical speeds for the 2 BHAs are shown in Figure 3.9 and Figure 3.10, respectively.

Table 3.8 Static BHA analysis for Manifa 6-1/8" hole (PWI well)

Well Properties			
Required WOB		20,000	lb
Mud Weight		9.759	ppg
BF		0.851	
Hole Inclination		90	°
MOP		30,000	lb

Drill Collar Design			
1	OD	0	in
	ID	0	in
	W_{dc}	0	lb/ft
	# of joints	0	
	L_{dc}	0	ft
2	OD	0	in
	ID	0	in
	W_{dc}	0	lb/ft
	# of joints	0	
	L_{dc}	0	ft
3	OD	0	in
	ID	0	in
	W_{dc}	0	lb/ft
	# of joints	0	
	L_{dc}	0	ft
SF		20%	
Weight applied by the BHA		0	lb

Drill Pipe Design			
Bottom Section	OD	4.000	in
	ID	3.340	in
	W_{dp}	14.00	lb/ft
	P_t(S135)	456,931	lb
	L_{dp}	32,004	ft
Top Section	OD	0	in
	ID	0	in
	W_{dp}	0	lb/ft
	P_t	0	lb
	L_{dp}	0	ft
BHA Submerged Load P		408,636	lb

Table 3.9 Dynamic data input for Manifa 6-1/8” hole BHA#1 (PWI well)

BHA#1: Manifa (6.125" hole section)						
String Geometry & Material						
BHA	Length (ft)	Cum Length (ft)	OD (in)	ID (in)	Weight (lb)	Material
6-1/8" BIT	0.73	0.7	6.125		500	Steel
AUTO TRAK	9.94	10.7	4.750	1.000	595	Steel
MWD STAB	2.70	13.4	4.750	1.500	220	Steel
BCPM2 (Baker)	10.77	24.1	4.750	2.000	922	Steel
MWD STAB	2.82	27.0	4.750	1.500	220	Steel
ON TRAK MWD	20.17	47.1	4.750	2.000	1,172	Steel
MWD STAB	2.42	49.6	4.750	1.500	200	Steel
LithoTrak	14.42	64.0	4.750	1.875	1,100	Steel
TEST TRAK	22.95	86.9	4.750	1.392	1,257	Steel
NM-STAB	5.20	92.1	4.750	1.500	275	Steel
MAGTRAK SENSOR	17.22	109.3	4.750	1.535	1,250	Steel
NM-STAB	4.83	114.2	4.750	1.500	275	Steel
NM SUB-STOP	1.62	115.8	4.750	2.000	150	Steel
DP-COMPRESSIVE	28.56	144.4	4.750	2.688	1,400	Steel
SUB-FLOAT	2.30	146.7	4.688	2.167	200	Steel
SUB-FILTER	6.02	152.7	4.750	2.688	400	Steel
SUB-X/O	3.00	155.7	4.750	2.000	400	Steel
1 X 4" HWDP	30.55	186.2	4.750	2.563	895	Steel
JAR	29.50	215.7	4.750	2.250	700	Steel
1 X 4" HWDP	30.59	246.3	4.750	2.563	896	Steel
960 X 4" DP	29,760.00	30,006.3	4.000	3.340	467,232	Steel
				Total Air Weight (lb)	**480,259**	
Borehole Geometry						
6.125"						
3D Well path						
Inclination	90°		Azimuth	344		
WOB (lb)						
20,000						
Mud Weight (ppg)						
9.759						

Table 3.10 Dynamic data input for Manifa 6-1/8” hole BHA#2 (PWI well)

BHA#2: Manifa (6.125" hole section)						
String Geometry & Material						
BHA	Length (ft)	Cum Length (ft)	OD (in)	ID (in)	Weight (lb)	Material
6-1/8" BIT	0.73	0.7	6.125		500	Steel
AUTO TRAK	9.94	10.7	4.750	1.000	595	Steel
MWD STAB	2.70	13.4	4.750	1.500	220	Steel
BCPM2 (Baker)	10.77	24.1	4.750	2.000	922	Steel
MWD STAB	2.82	27.0	4.750	1.500	220	Steel
ON TRAK MWD	20.17	47.1	4.750	2.000	1,172	Steel
MWD STAB	2.42	49.6	4.750	1.500	200	Steel
LithoTrak	14.42	64.0	4.750	1.875	1,100	Steel
TEST TRAK	22.95	86.9	4.750	1.392	1,257	Steel
NM-STAB	5.20	92.1	4.750	1.500	275	Steel
MAGTRAK SENSOR	17.22	109.3	4.750	1.535	1,250	Steel
NM-STAB	4.83	114.2	4.750	1.500	275	Steel
NM SUB-STOP	1.62	115.8	4.750	2.000	150	Steel
DP-COMPRESSIVE	28.56	144.4	4.750	2.688	1,400	Steel
SUB-FLOAT	2.30	146.7	4.688	2.167	200	Steel
SUB-FILTER	6.02	152.7	4.750	2.688	400	Steel
SUB-X/O	3.00	155.7	4.750	2.000	400	Steel
7 X 4" HWDP	210.00	365.7	4.750	2.563	6,153	Steel
JAR	29.50	395.2	4.750	2.250	700	Steel
7 X 4" HWDP	210.00	605.2	4.750	2.563	6,153	Steel
948 X 4" DP	29,388.00	29,993.2	4.000	3.340	461,392	Steel
				Total Air Weight (lb)	**484,934**	
Borehole Geometry						
6.125"						
3D Well path						
Inclination	90°		Azimuth	344		
WOB (lb)						
20,000						
Mud Weight (ppg)						
9.759						

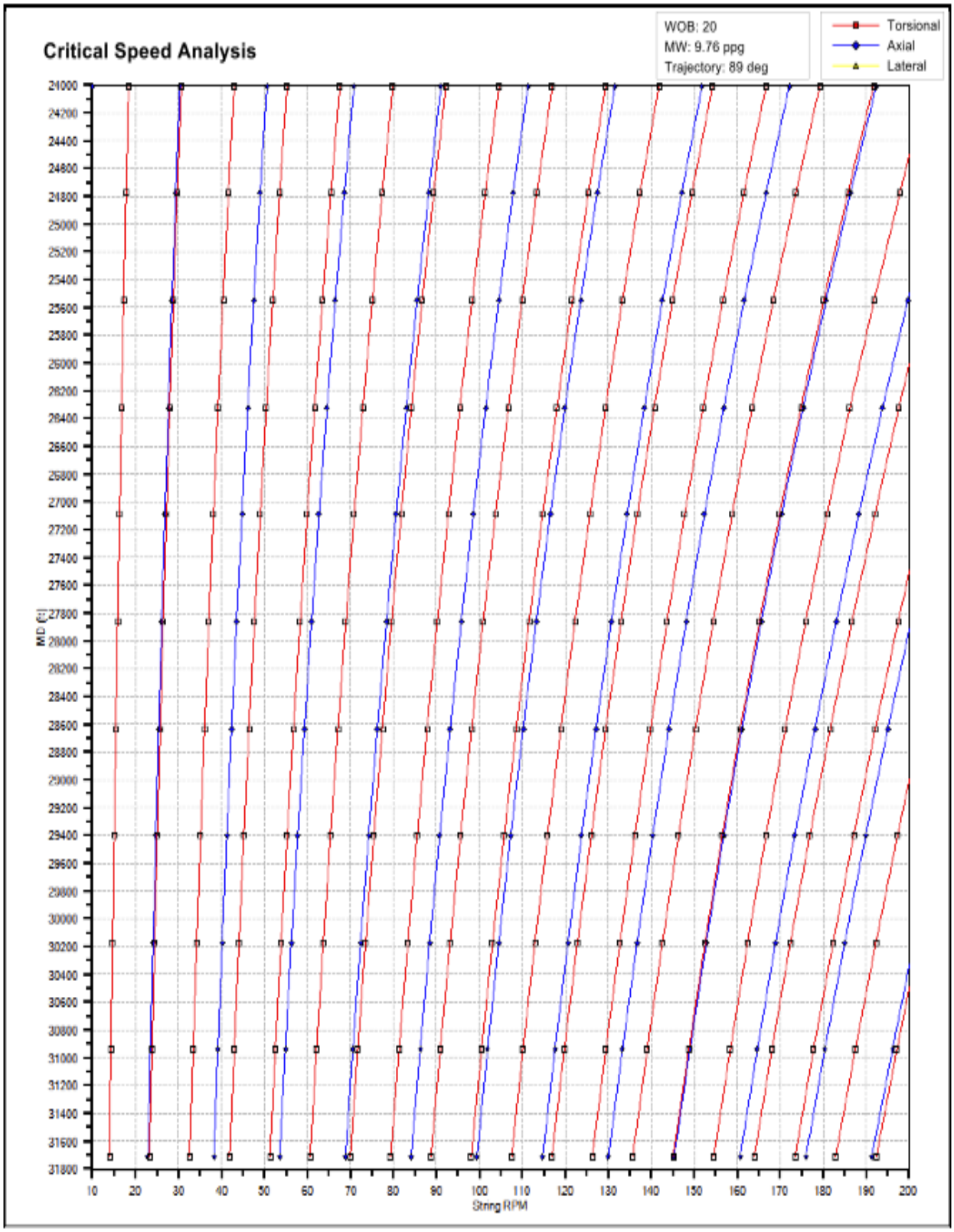

Figure 3.9 Critical speeds for Manifa 6-1/8” hole BHA#1

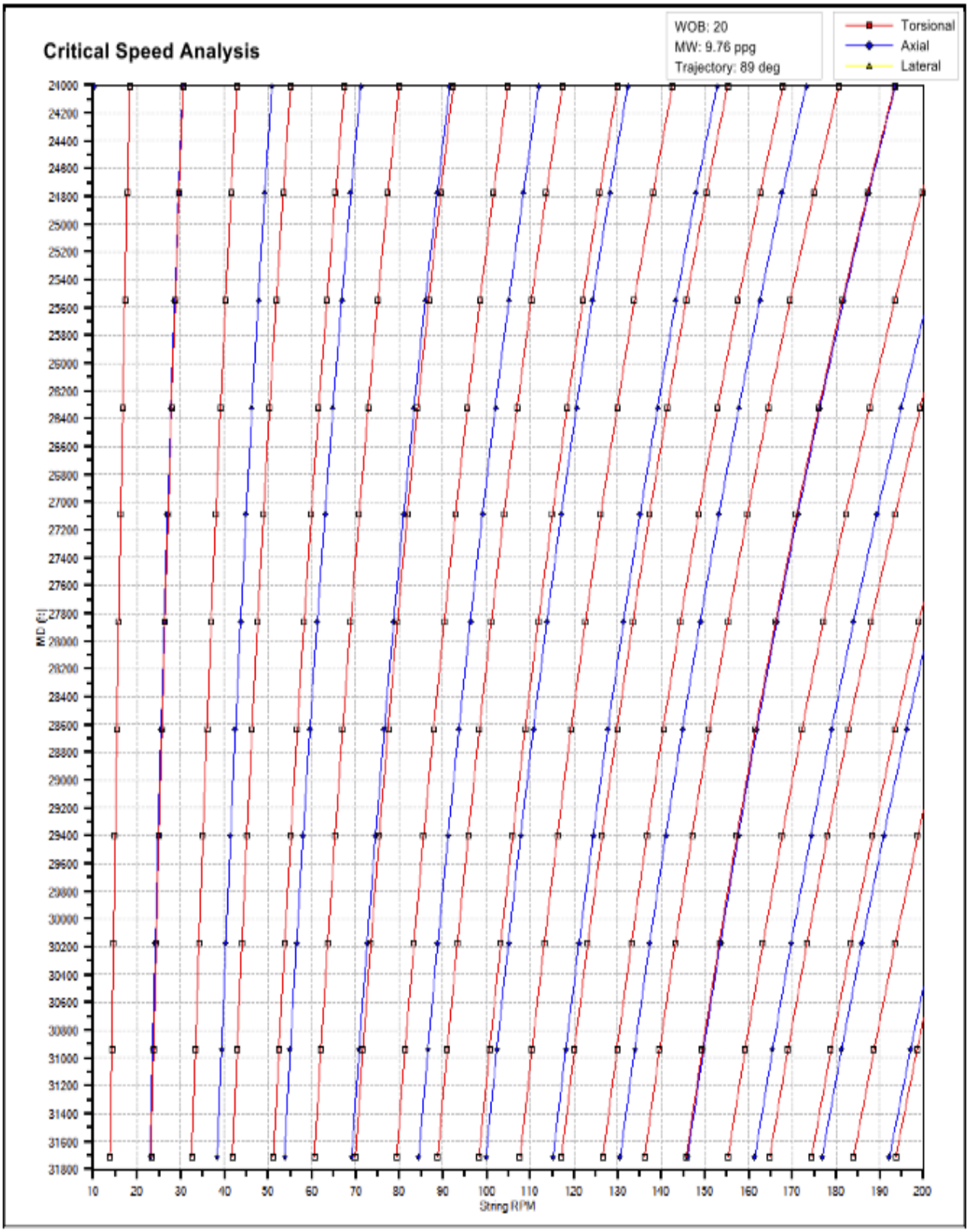

Figure 3.10 Critical speeds for Manifa 6-1/8” hole BHA#2

The critical speed chart for the 6-1/8” hole section BHA#1 in Figure 3.9 shows the difficulty of drilling in extended reach horizontal applications. The range of safe rotary speed is very small. It can be seen from the graph that the range is mostly straight line in the small rotary speeds (up to 90 RPM) and gets more curvy when the rotary speed increases. The unusually long section, drilled horizontally across the Lower Ratawi reservoir, will definitely result in downhole vibration and/or torque and drag issues. The dilemma here is to have a balance between reducing the vibration and at the same time run a slick assembly that would minimize the downhole torque that is associated with ERD horizontal drilling. Drill collars were intentionally eliminated from this section to reduce the possibility of stuck pipe and were replaced by HWDP.

BHA#2 is proposed as an alternative to BHA#1. Seven 4-3/4” HWDP were placed below the mechanical jar and seven 4-3/4” HWDP were placed above the jar. The addition of HWDP will lead to an increase in the weight and the stiffness and thus may reduce the vibration levels. There are no difference between the speed range of BHA#1 and BHA#2 as shown in Figure 3.9 and Figure 3.10,respectively. The reason behind this is the abnormally long drillstring of this hole section. It can be noticed that lateral vibration is not present in both models.

4. CASE STUDY: KARAN FIELD

Karan field, discovered in 2006, is a non-associated offshore gas field that is located about 100 miles north of Dhahran as shown in Figure 4.1 (SaudiAramco 2010). 21 producer wells will be drilled over 5 offshore wellhead platforms (SaudiAramco 2010). The project will deliver 1.8 billion scfd of raw gas through 68 miles of subsea pipelines to Khursaniyah gas plant when it is completed in 2012 (SaudiAramco 2010). The Khuff carbonate formation is the targeted reservoir, which has a thickness around 1000 ft (Canty 2011). Figure 4.2 shows a schematic of a Karan well that will be analyzed in this chapter.

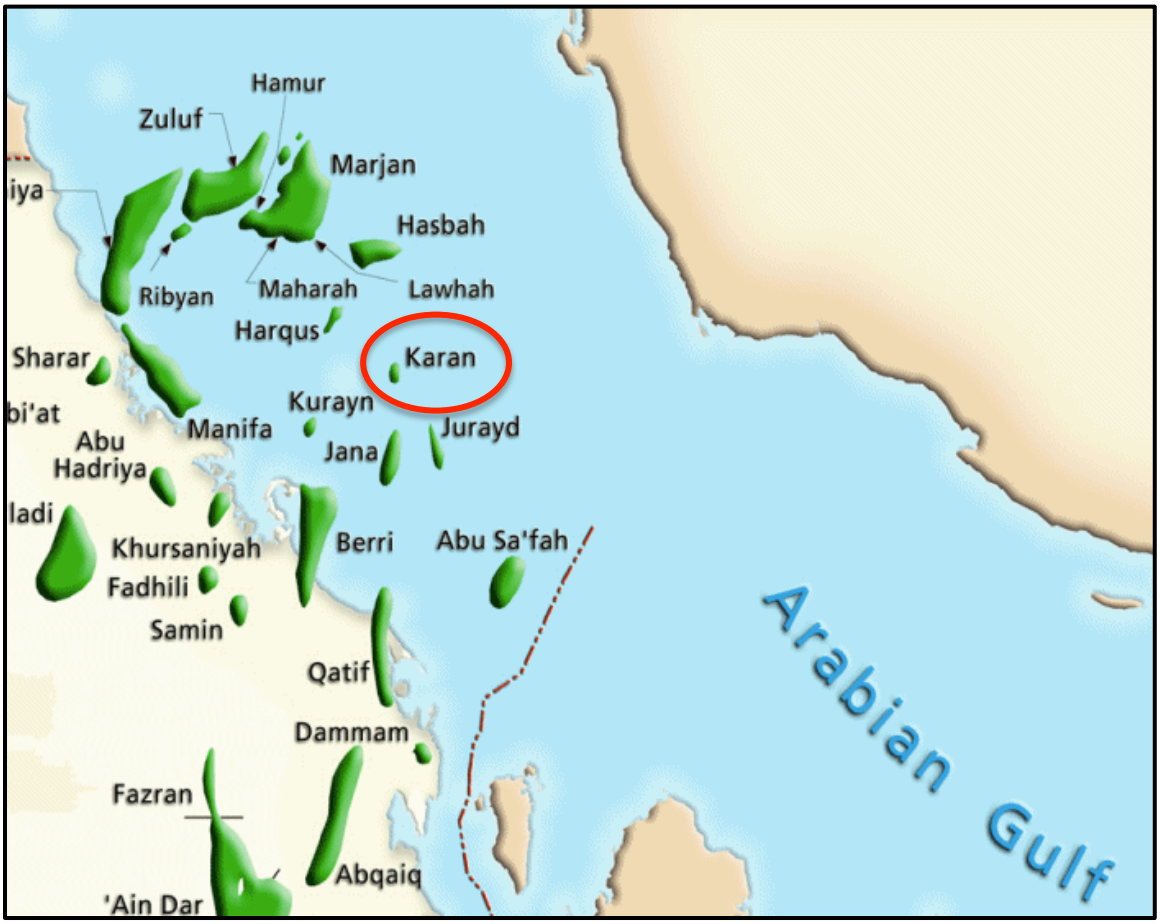

Figure 4.1 Karan gas field location on the Arabian Gulf (source: Saudi Aramco)

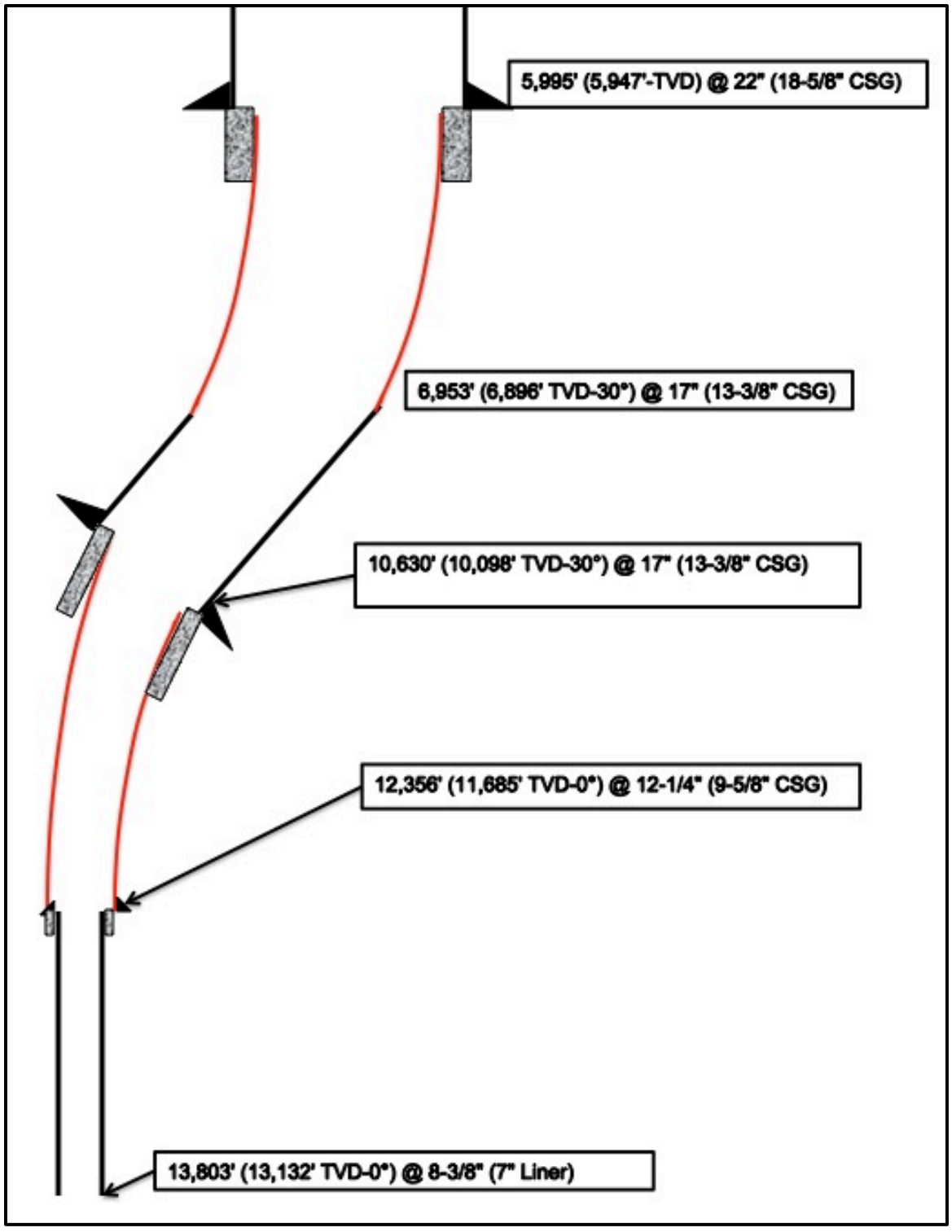

Figure 4.2 A schematic for a Karan well

4.1. Karan 17” Hole (Gas Producer)

This hole section was drilled from 6,000’ MD (5,947’ TVD – 0° inclination) to 13-3/8” casing point at 10,630’ MD (10,100’ TVD – 30° inclination). This casing is intended to shut off possible lost circulation intervals and H_2S gas. BHA#1 properties are shown in Table 4.1 and Table 4.2. 2 non-magnetic drill collars were run to separate MWD and were neglected in the static design. Critical speeds of this BHA configuration is shown in Figure 4.3.

Table 4.1 Static BHA analysis for Karan 17” hole (gas producer)

Well Properties							
Required WOB				40,000	lb		
Mud Weight				10.694	ppg		
BF				0.837			
Hole Inclination				30	°		
MOP				100,000	lb		
Drill Collar Design				**Drill Pipe Design**			
1	OD	9.500	in	Bottom Section	OD	5.500	in
	ID	3.000	in		ID	4.670	in
	W_{dc}	216	lb/ft		W_{dp}	24.7	lb/ft
	# of joints	4			P_t (E75)	391,285	lb
	L_{dc}	125.5	ft		L_{dp}	10,345	ft
2	OD	8.25	in	Top Section	OD	0	in
	ID	2.88	in		ID	0	in
	W_{dc}	160	lb/ft		W_{dp}	0	lb/ft
	# of joints	5			P_t	0	lb
	L_{dc}	155.5	ft		L_{dp}	0	ft
SF		20%		BHA Submerged Load P		282,836	lb
Weight applied by the BHA		57,574	lb				

Table 4.2 Dynamic data input for Karan 17” hole BHA#1 (gas producer)

BHA#1: Karan (17" hole section)						
String Geometry & Material						
BHA	Length (ft)	Cum Length (ft)	OD (in)	ID (in)	Weight (lb)	Material
17" bit	1.90	1.9	17.000		500	Steel
PowerPak A92GT	31.41	33.3	9.625	7.850	6,350	Steel
Float Sub	3.15	36.5	9.620	4.750	400	Steel
15-3/4" IBS	8.40	44.9	9.560	3.000	4,000	Steel
9-1/2" Pony NMDC	14.90	59.8	9.630	3.000	3,218	Steel
Saver Sub	1.15	60.9	9.170	3.500	200	Steel
PowePulse	24.91	85.8	9.130	6.250	3,100	Steel
Saver Sub	1.90	87.7	9.560	3.500	200	Steel
9-1/2" NMDC	31.46	119.2	9.580	3.060	6,795	Steel
3 X 9-1/2" Drill Collar	94.00	213.2	9.500	3.000	20,304	Steel
XO	4.44	217.6	8.500	3.000	650	Steel
3 X 8-1/4" Drill Collar	93.00	310.6	8.250	3.000	14,694	Steel
Mechanical Jar	33.67	344.3	8.000	3.000	2,200	Steel
2 X 8-1/4" Drill Collar	62.50	406.8	8.250	2.880	10,000	Steel
XO	2.60	409.4	8.130	3.000	550	Steel
12 X 5-1/2" HWDP	369.00	778.4	5.500	3.250	22,199	Steel
317 X 5-1/2" DP	9,827.00	10,605.4	5.500	4.670	242,727	Steel
				Total Air Weight (lb)	**338,088**	
Borehole Geometry						
17"						
3D Well path						
Inclination	29°		Azimuth	27		
WOB (lb)						
40,000						
Mud Weight (ppg)						
10.694						

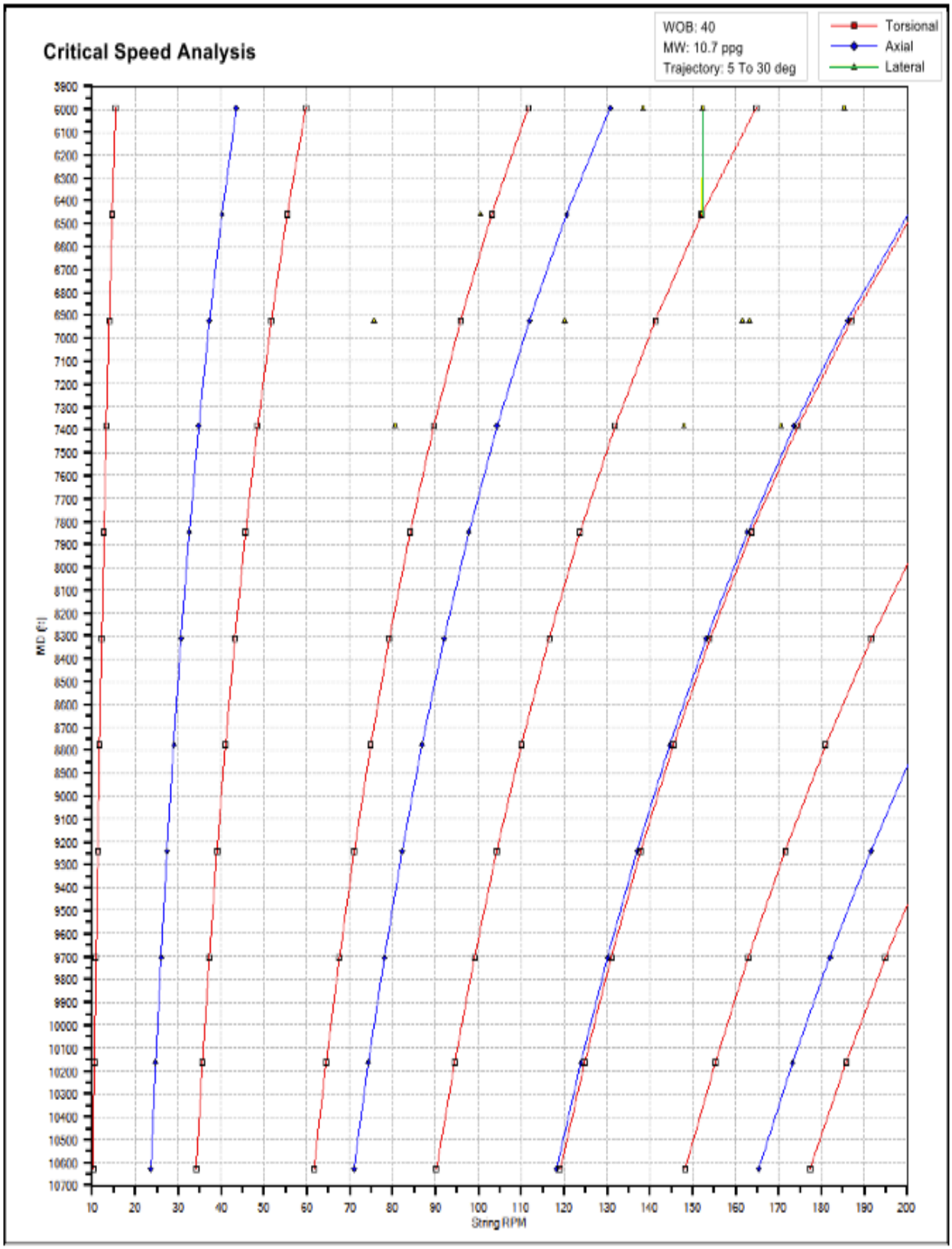

Figure 4.3 Critical speeds for Karan 17” hole BHA#1

The critical speed chart for the 17” hole section in Figure 4.3 shows a good safe operating range. It can be seen that the ranges are very wide due to running multiple segments of drill collars, which will add extra stiffness to the drillstring and minimize vibration. Lateral vibration will occur only on the top portion for around 500 ft, where the build section will start from 0 - 30°. Moreover, the short drilling section (4,600 ft) will allow better vibration management of this section.

4.2. Karan 12-1/4” Hole (Gas Producer)

This hole section was drilled from 10,630’ MD (10,100’ TVD – 30° inclination) to the 9-5/8” casing point at 12,360’ MD (11,685’ TVD – 0° inclination). The purpose of this casing is to stop abnormal gas or saltwater flow and avoid possible tight hole/swelling shale. BHA#1 properties are shown in Table 4.3 and Table 4.4. BHA#2 configuration is presented in Table 4.5. Critical speeds for both BHAs are shown in Figure 4.4 and Figure 4.5, respectively.

Table 4.3 Static BHA analysis for Karan 12-1/4" hole (gas producer)

Well Properties							
Required WOB				25,000	lb		
Mud Weight				17.913	ppg		
BF				0.726			
Hole Inclination				0	°		
MOP				100,000	lb		
Drill Collar Design				**Drill Pipe Design**			
1	OD	8.25	in	Bottom Section	OD	5.500	in
	ID	2.813	in		ID	4.670	in
	W_{dc}	160	lb/ft		W_{dp}	24.7	lb/ft
	# of joints	4			P_t (E75)	391,285	lb
	L_{dc}	120	ft		L_{dp}	13,270	ft
2	OD	0	in	Top Section	OD	0	in
	ID	0	in		ID	0	in
	W_{dc}	0	lb/ft		W_{dp}	0	lb/ft
	# of joints	0			P_t	0	lb
	L_{dc}	0	ft		L_{dp}	0	ft
SF		20%		BHA Submerged Load P		269,743	lb
Weight applied by the BHA (lb)		19,427	lb				

Table 4.4 Dynamic data input for Karan 12-1/4” hole BHA#1 (gas producer)

BHA#1: Karan (12.25" hole section)						
String Geometry & Material						
BHA	Length (ft)	Cum Length (ft)	OD (in)	ID (in)	Weight (lb)	Material
12" PDC Bit	1.20	1.2	12.000		200	Steel
PowerDrive 900 X5	13.80	15.0	9.000	5.125	2,500	Steel
Stabilized Receiver Sub	5.95	21.0	8.400	3.750	900	Steel
Saver Sub	1.77	22.7	8.400	3.750	200	Steel
PowerPulse 825 HF	24.60	47.3	8.250	5.900	3,100	Steel
Saver Sub	1.50	48.8	8.250	3.750	200	Steel
PBL Sub	9.00	57.8	7.880	3.000	1,300	Steel
2 x 8-1/4" DC	60.00	117.8	8.250	2.813	9,600	Steel
8" Hydraulic Jar	31.32	149.1	8.125	3.000	3,900	Steel
2 x 8-1/4" DC	60.00	209.1	8.250	2.813	9,600	Steel
Crossover	3.78	212.9	8.500	2.875	600	Steel
36 x 5-1/2" HWDP	1,109.16	1,322.1	5.500	3.250	66,727	Steel
356 X 5-1/2" DP	11,036. 0	12,358.1	5.500	4.670	272,589	Steel
				Total Air Weight (lb)	**317,416**	
Borehole Geometry						
12.25"						
3D Well path						
Inclination	0°		Azimuth	27		
WOB (lb)						
25,000						
Mud Weight (ppg)						
17.913						

Table 4.5 Dynamic data input for Karan 12-1/4” hole BHA#2 (gas producer)

BHA#2: Karan (12.25" hole section)						
String Geometry & Material						
BHA	Length (ft)	Cum Length (ft)	OD (in)	ID (in)	Weight (lb)	Material
12" PDC Bit	1.20	1.2	12.000		200	Steel
PowerDrive 900 X5	13.80	15.0	9.000	5.125	2,500	Steel
Stabilized Reciever Sub	5.95	21.0	8.400	3.750	900	Steel
Saver Sub	1.77	22.7	8.400	3.750	200	Steel
PowerPulse 825 HF	24.60	47.3	8.250	5.900	3,100	Steel
Saver Sub	1.50	48.8	8.250	3.750	200	Steel
PBL Sub	9.00	57.8	7.880	3.000	1,300	Steel
4 x 8-1/4" DC	120.00	177.8	8.250	2.813	19,200	Steel
8" Hydraulic Jar	31.32	209.1	8.125	3.000	3,900	Steel
4 x 8-1/4" DC	120.00	329.1	8.250	2.813	19,200	Steel
Crossover	3.78	332.9	8.500	2.875	600	Steel
32 x 5-1/2" HWDP	985.16	1,318.1	5.500	3.250	59,267	Steel
356 X 5-1/2" DP	11,036.00	12,354.1	5.500	4.670	272,589	Steel
				Total Air Weight (lb)	**383,156**	
Borehole Geometry						
12.25"						
3D Well path						
Inclination	0°		Azimuth	27		
WOB (lb)						
25,000						
Mud Weight (ppg)						
17.913						

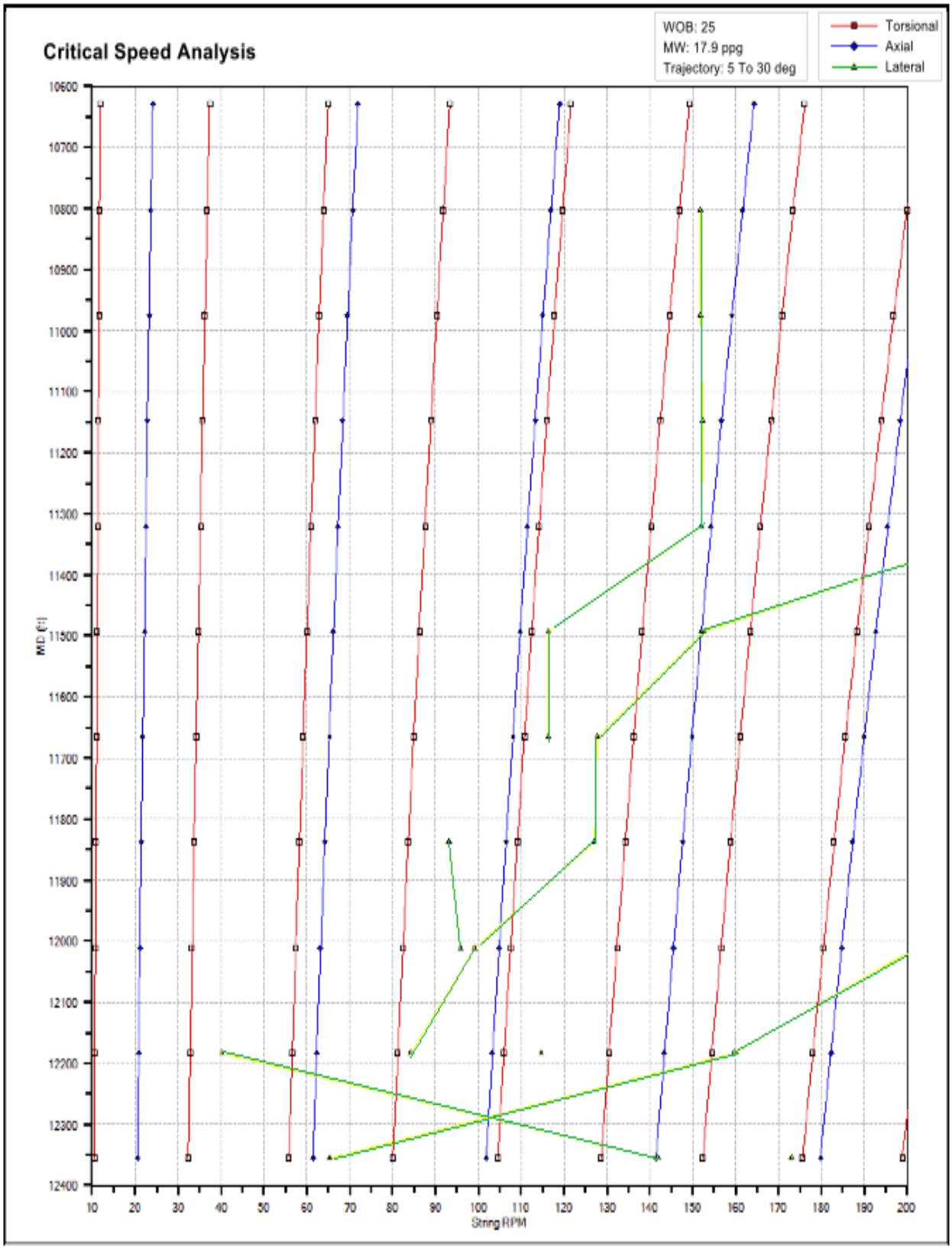

Figure 4.4 Critical speeds of Karan12-1/4” hole BHA#1

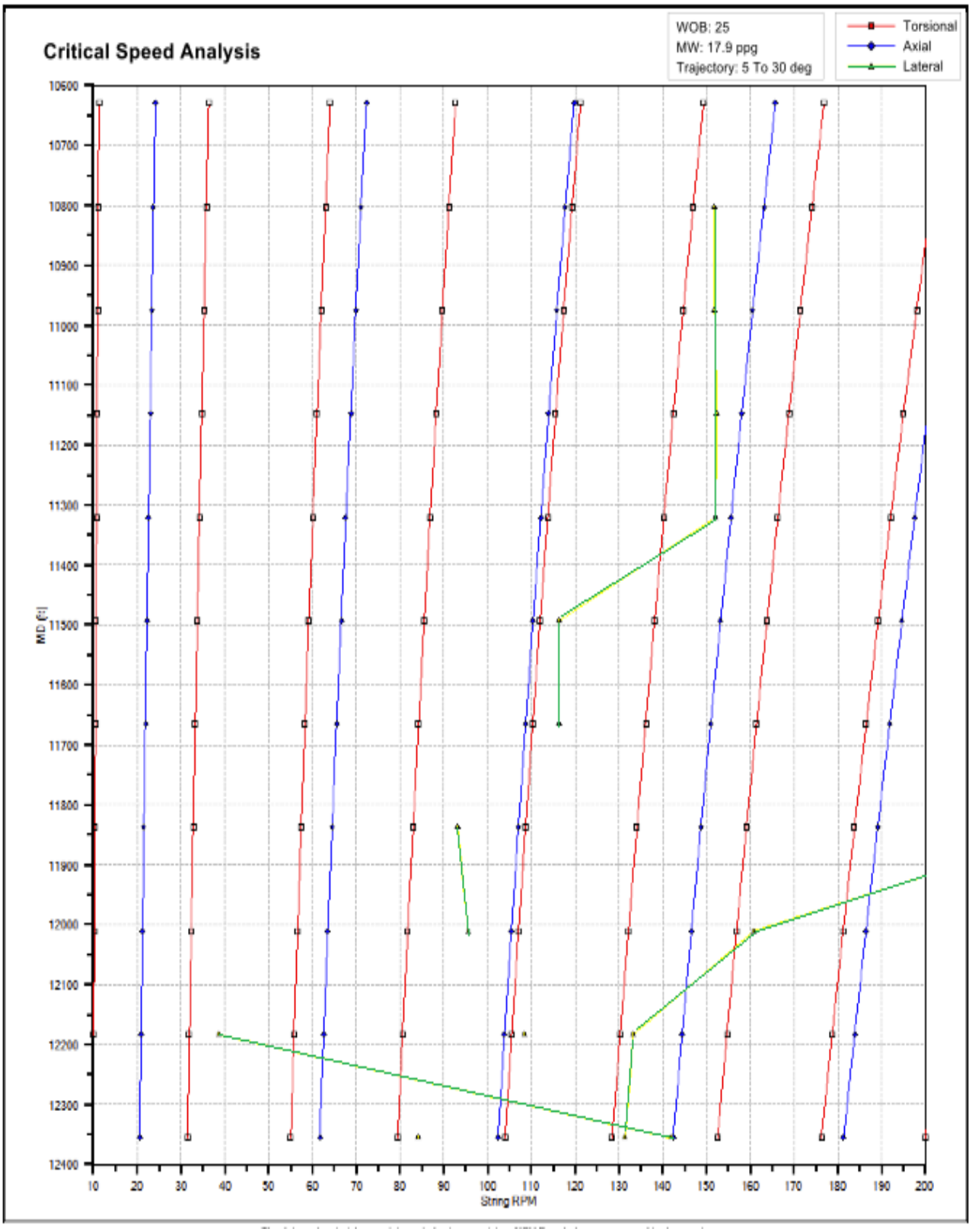

Figure 4.5 Critical speeds of Karan12-1/4” hole BHA#2

BHA#1 critical speed chart is shown in Figure 4.4. This section is considered to be a short section since only 1,800 ft will be drilled. The reason for drilling such a short section is due to possible saltwater flow and/or abnormal gas pressure in these formations. From the graph, it is suggested to stay between 60-80 RPM. At depth around 12,200 ft, the lateral vibration could not be avoided for all speeds as can seen in the graph. It is believed that the inclination drop from 30-0° may lead to this problem although it is a short drilling section. As the inclination approaches zero, the possibility of encountering lateral vibration increases.

BHA#2 was proposed in Table 4.5 by increasing the number of drill collar joints and decreasing the HWDP. Four 8-1/2” drill collar joints are placed below the jar and another four joints are placed above the jar. The HWDP joints were reduced to 32 joints instead of 36 joints. The increase in drill collar joints lead to improvement in the critical speed range as appears in Figure 4.5. Lateral vibration (colored in green) has been eliminated in many depth segments in the redesigned BHA. Axial and torsional vibration speed ranges have not changed that much in both BHAs.

4.3. Karan 8-3/8" Hole (Gas Producer)

This hole section was drilled from 12,360' MD (11,685' TVD – 0° inclination) to the 7" perforated liner at 13,800' MD (13,132' TVD – 0° inclination). BHA#1 properties are shown in Table 4.6 and Table 4.7. BHA#2 properties are presented in Table 4.8. Critical speeds for BHA#1 and BHA#2 are presented in Figure 4.6 and Figure 4.7, respectively.

Table 4.6 Static BHA analysis for Karan 8-3/8" hole (gas producer)

Well Properties			
Required WOB		25,000	lb
Mud Weight		15.240	ppg
BF		0.767	
Hole Inclination		0	°
MOP		100,000	lb

Drill Collar Design			
1	OD	6.500	in
	ID	3.000	in
	W_{dc}	88.86	lb/ft
	# of joints	18	
	L_{dc}	541.61	ft
2	OD	0	in
	ID	0	in
	W_{dc}	0	lb/ft
	# of joints	0	
	L_{dc}	0	ft
3	OD	0	in
	ID	0	in
	W_{dc}	0	lb/ft
	# of joints	0	
	L_{dc}	0	ft
SF		20%	
Weight applied by the BHA (lb)		34,819	lb

Drill Pipe Design			
Bottom Section	OD	4.000	in
	ID	3.340	in
	W_{dp}	14	lb/ft
	P_t	313,854	lb
	L_{dp}	14,793	ft
Top Section	OD	5.500	in
	ID	4.670	in
	W_{dp}	24.7	lb/ft
	P_t	547,799	lb
	L_{dp}	11,112	ft
BHA Submerged Load P		277,175	lb

Table 4.7 Dynamic data input for Karan 8-3/8” hole BHA#1 (gas producer)

BHA#1: Karan (8.375" hole section)						
String Geometry & Material						
BHA	Length (ft)	Cum Length (ft)	OD (in)	ID (in)	Weight (lb)	Material
8-3/8" PDC Bit	0.84	0.8	8.375		120	Steel
Stabilizer (reamer)	5.48	6.3	6.500	2.250	453	Steel
Float Sub	3.00	9.3	4.440	2.160	122	Steel
XO	3.00	12.3	6.250	2.750	250	Steel
1 X 6-1/2" Drill Collar	30.02	42.3	6.500	3.000	2,668	Steel
Stabilizer (reamer)	7.14	49.5	6.250	2.000	647	Steel
2 X 6-1/2" Drill Collar	61.40	110.9	6.500	3.000	5,456	Steel
Mechanical Jar	31.45	142.3	6.500	2.750	4,280	Steel
15 X 6-1/2" Drill Collar	450.19	592.5	6.500	3.000	40,004	Steel
Sub	5.71	598.2	6.500	3.813	469	Steel
130 X 4" HWDP	390.00	988.2	4.000	2.500	11,977	Steel
66 X 4" Drill Pipe	2,000.00	2,988.2	4.000	3.340	28,000	Steel
Sub	3.00	2,991.2	4.440	2.160	122	Steel
360 X 5-1/2" Drill Pipe	10,800.0	13,791.2	5.500	4.670	266,760	Steel
				Total Air Weight (lb)	**361,327**	
Borehole Geometry						
8.375"						
3D Well path						
Inclination	0°		Azimuth	27		
WOB (lb)						
25,000						
Mud Weight (ppg)						
15.240						

Table 4.8 Dynamic data input for Karan 8-3/8” hole BHA#2 (gas producer)

BHA#2: Karan (8.375" hole section)						
String Geometry & Material						
BHA	Length (ft)	Cum Length (ft)	OD (in)	ID (in)	Weight (lb)	Material
8-3/8" PDC Bit	0.84	0.8	8.375		120	Steel
Stabilizer (reamer)	5.48	6.3	6.500	2.250	453	Steel
Float Sub	3.00	9.3	4.440	2.160	122	Steel
XO	3.00	12.3	6.250	2.750	250	Steel
1 X 6-1/2" Drill Collar	30.02	42.3	6.500	3.000	2,668	Steel
Stabilizer (reamer)	7.14	49.5	6.250	2.000	647	Steel
2 X 6-1/2" Drill Collar	61.40	110.9	6.500	3.000	5,456	Steel
Mechanical Jar	31.45	142.3	6.500	2.750	4,280	Steel
11 X 6-1/2" Drill Collar	330.00	472.3	6.500	3.000	29,324	Steel
Sub	5.71	478.0	6.500	3.813	469	Steel
134 X 4" HWDP	510.00	988.0	4.000	2.500	15,662	Steel
66 X 5" Drill Pipe	2,000.00	2,988.0	5.000	4.276	39,000	Steel
Sub	3.00	2,991.0	4.440	2.160	122	Steel
360 X 5-1/2" Drill Pipe	10,800.0	13,791.2	5.500	4.670	266,760	Steel
				Total Air Weight (lb)	**365,332**	
Borehole Geometry						
8.375"						
3D Well path						
Inclination	0°		Azimuth	27		
WOB (lb)						
25,000						
Mud Weight (ppg)						
15.240						

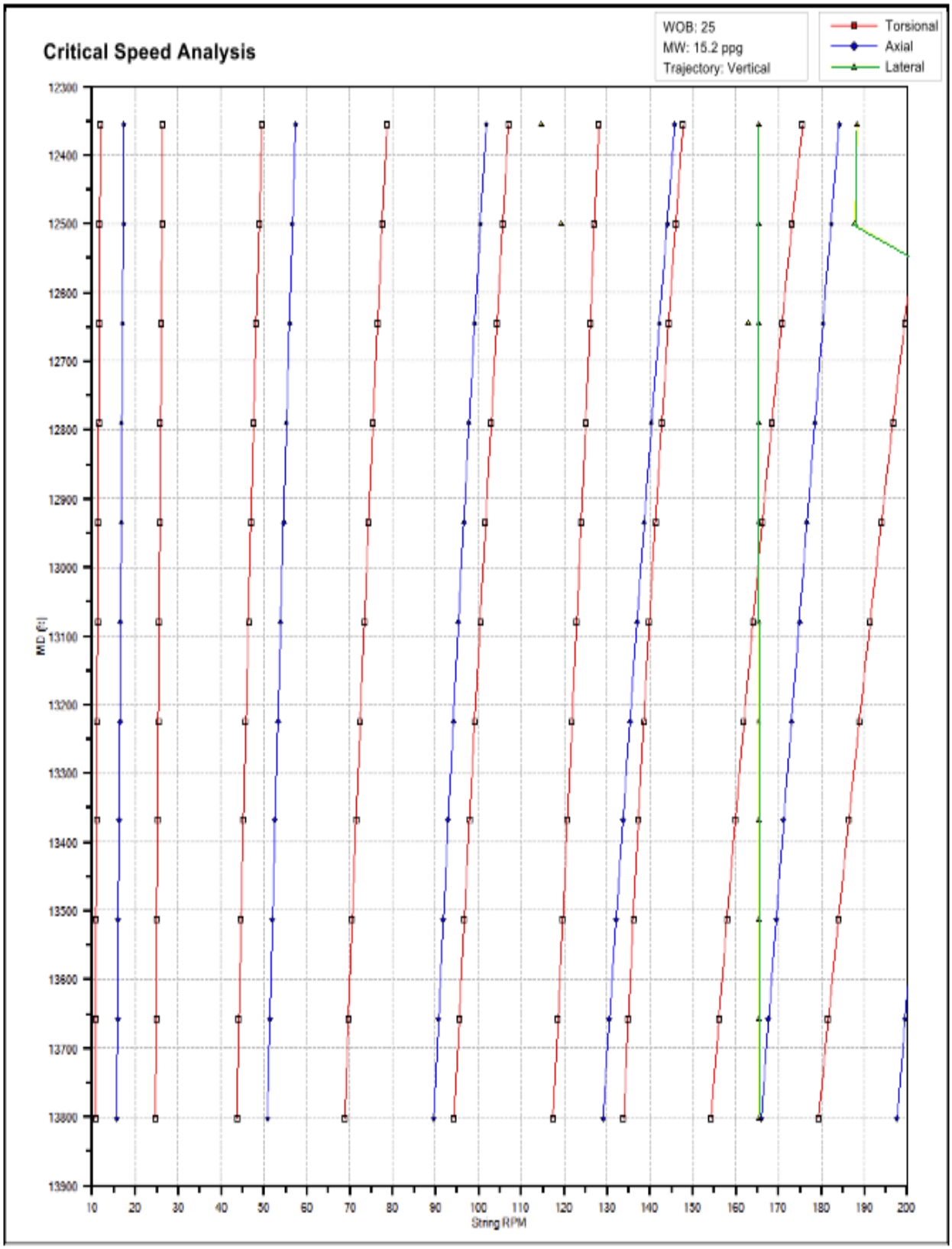

Figure 4.6 Critical speeds of Karan 8-3/8” hole BHA#1

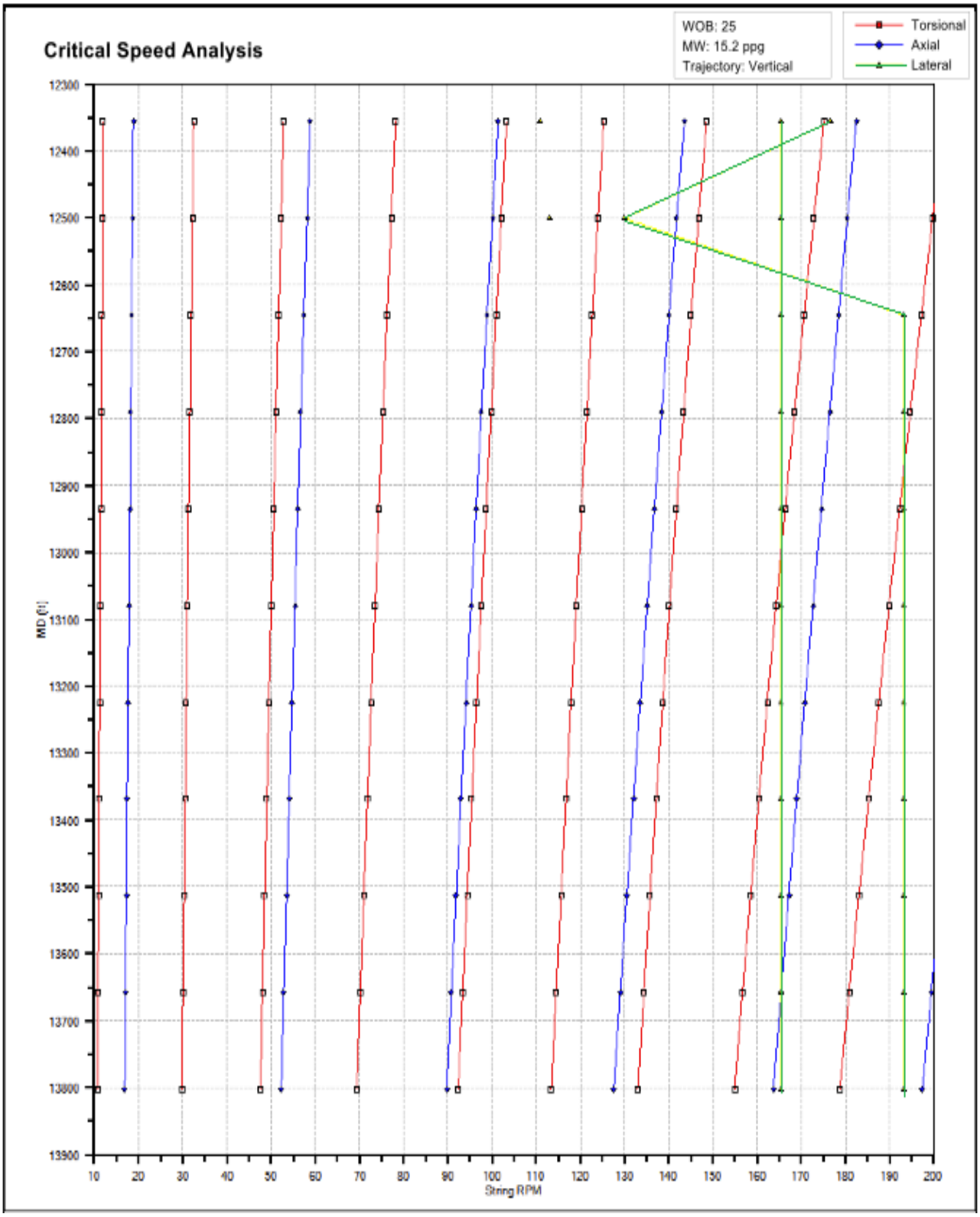

Figure 4.7 Critical speeds of Karan 8-3/8” hole BHA#2

This hole section was drilled using the rotary mode instead of downhole motors since it will be vertical section. This 8-3/8” hole section was drilled across the thick Khuff carbonate reservoir with depth that can reach 1,000 ft. BHA#1 details are tabulated in Table 4.7. The critical speed analysis for BHA#1 is shown in Figure 4.6. The safe operating range is quite good for this hole section. It is recommended to install a shock sub to minimize the axial drilling vibration since the section will be drilled vertically in carbonate rock formation. Lateral vibration will occur at very high speed i.e. 165, which would not be a critical problem.

BHA#2 is a modification from the original BHA as shown in Table 4.8. Drill collar joints were reduced to eleven 6-1/2” drill collar joints (instead of 15) and HWDP joints were increased to 134 joints. Moreover, the first drill pipe segment size was changed to 5” drill pipe (instead of 4” drill pipe in the original design) in a try to decrease the abrupt change in the outer diameter. The comparison between critical speed ranges for BHA#1 and BHA#2, as shown in Figure 4.6 and Figure 4.7, shows that the critical speed range for axial and torsional vibration is better for the first BHA (BHA#1). Moreover, lateral vibration spikes are present in BHA#2 when the drill collar joints were reduced suggesting that the presence of drill collars in the vertical section will greatly help to avoid lateral vibration.

5. CONCLUSION

This thesis aims to provide more investigation in understanding the downhole vibration in a qualitative manner. Two oil and gas fields case studies were analyzed in this thesis. These fields are Manifa oil field and Karan non-associated gas field, which are both being developed by Saudi Aramco. The drillstring critical speed analysis is an important factor to be analyzed in order to reduce the risk associated with downhole vibration. Different BHAs configurations are analyzed to select the best one that corresponds to a wider safe operating speed range for a certain hole section.

The analysis is based on the FEA approach, where the drillstring is modeled as discretized mesh of a long-body system. The software program that was used to model those BHA configurations is Vibrascope™.

The BHA harmonic analysis of Manifa oil field showed that the upper big hole section (12-1/4” hole) has a good range of operating speed. However, the situation gets worse when drilling the small hole sections (8-1/2” and 6-1/8” hole) since the drilled sections are very long (13,000 ft and 8,000 ft respectively). Increasing the stiffness (and weight) was proposed as a solution to obtain better results in terms of operating speed. This solution has not lead to improvement in term of critical speed range. It is believed that the effect of the super long drill string has much greater factor in vibration control than that of stiffness.

For Karan gas field, the 17” hole build section showed good operating speed range. For 12-1/4” hole, the section will drop the angle from 30 – 0°

inclination. This led to the presence of lateral vibration especially when approaching to 0° inclination. Increasing the drill collar section led to improving the critical speed range and eliminating lateral vibration in multiple sections. The 8-3/8" reservoir hole section critical speed range is quite good. It is highly recommended to run a shock sub in this section since it is a long vertical section that will be drilled in hard formations. Decreasing the number of drill collar joints and increasing the HWDP in BHA#2 made the situation worse by introducing more lateral vibration sections.

Limitations:

One of the limitation of this study is that it does not investigate the shear load and displacement as a function of rotary speed (RPM). The importance of those parameters arises from ability of a drilling engineer to determine the critical points of the BHA that can lead to fatigue breakage or high fluctuation. Also, the rock type is an important factor that need to be studied since it has high impact on the drilling vibration. Another limitation is that the post-well analysis should be compared with real downhole data to validate the analysis.

Recommendation:

To improve future work, possible lost circulation zones should be considered since there will be no fluid outside the drillstring, which may reduce the viscous damping ratios. Moreover, the presence of swelling shale, abnormal gas pressure, and salt domes may worth additional analysis. Finally, downhole shock recorders are recommended to be run, especially in ERD wells. This will

help in understanding the behavior of vibration problems as more extended reach projects are expected in next years.

APPENDICES

A. Damped Simple Harmonic Motion

An ideal mass–spring–damper system with mass m (kg), spring constant k (N/m) and viscous damper of damping coefficient c (N.sec/m or kg/sec) is subject to an oscillatory force F_s

$$F_s = -kx \qquad \text{(eq A.1)}$$

a damping force F_d

$$F_d = -cv = -c\frac{dx}{dt} = -c\dot{x} \qquad \text{(eq A.2)}$$

Treating the mass as a free body and applying Newton's second law, the total force F_{total} on the body is

$$F_{total} = ma = m\frac{d^2x}{dt^2} = m\ddot{x} \qquad \text{(eq A.3)}$$

where a is the acceleration (m/s^2) of the mass and x is the displacement (m) of the mass relative to a fixed point of reference.

Since $F_{total} = F_s + F_d$,

$$m\ddot{x} = -kx - c\dot{x} \qquad \text{(eq A.4)}$$

This differential equation may be rearranged into

$$\ddot{x} + \frac{c}{m}\dot{x} + \frac{k}{m}x = 0 \qquad \text{(eq A.5)}$$

The following parameters are then defined:

$$\omega_0 = \sqrt{\frac{k}{m}} \qquad \text{(eq A.6)}$$

$$\zeta = \frac{c}{2\sqrt{mk}} \qquad \text{(eq A.7)}$$

The first parameter, ω_0, is called the (un-damped) natural frequency of the system. The second parameter, ζ, is called the damping ratio. The natural frequency represents an angular frequency, expressed in radians per second. The damping ratio is a dimensionless quantity.

The differential equation now becomes

$$\ddot{x} + 2\zeta\omega_0\dot{x} + \omega_0^2 x = 0 \qquad \text{(eq A.8)}$$

The equation can be solved by assuming a solution x such that:

$$x = e^{\gamma t} \qquad \text{(eq A.9)}$$

where the parameter γ (gamma) is, in general, a complex number.

Substituting this assumed solution back into the differential equation gives

$$\gamma^2 + 2\zeta\omega_0\gamma + \omega_0^2 x = 0 \qquad \text{(eq A.10)}$$

which is the characteristic equation.

Solving the characteristic equation will give two roots, γ_+ and γ_-. The solution to the differential equation is thus

$$x(t) = Ae^{\gamma_+ t} + Be^{\gamma_- t} \qquad \text{(eq A.11)}$$

where A and B are determined by the initial conditions of the system:

$$A = x(0) + \frac{\gamma_- x(0) - \dot{x}(0)}{\gamma_- - \gamma_+} \qquad \text{(eq A.12)}$$

$$B = -\frac{\gamma_- x(0) - \dot{x}(0)}{\gamma_- - \gamma_+} \qquad \text{(eq A.13)}$$

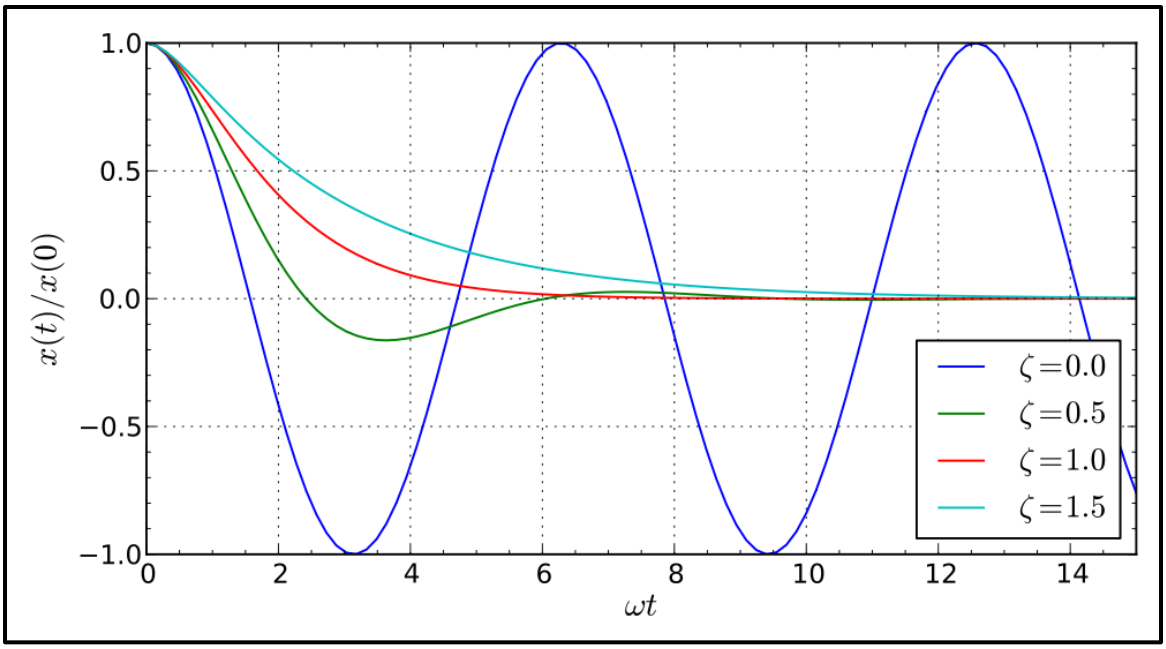

Figure B.1 System behavior for different damping ratio ζ: un-damped (blue), under-damped (green), critically damped (red), and over-damped (cyan) cases, for zero-velocity initial condition (source: Wikipedia).

The behavior of the system depends on the relative values of the two fundamental parameters, the natural frequency ω_0 and the damping ratio ζ. In particular, the qualitative behavior of the system depends crucially on whether the quadratic equation for γ has one real solution, two real solutions, or two complex conjugate solutions.

Critical damping (ζ = 1)

When ζ = 1, there is a double root γ (defined above), which is real. The system is said to be critically damped. A critically damped system converges to zero as fast as possible without oscillating. An example of critical damping is the door closer seen on many hinged doors in public buildings. The recoil mechanisms in most

guns are also critically damped so that they return to their original position, after the recoil due to firing, in the least possible time.

Over damping ($\zeta > 1$)

When $\zeta > 1$, the system is over-damped and there are two different real roots. An over-damped door-closer will take longer to close than a critically damped door would.

Under-damping ($0 \leq \zeta < 1$)

Finally, when $0 \leq \zeta < 1$, γ is complex, and the system is under-damped. In this situation, the system will oscillate at the natural damped frequency ω_d, which is a function of the natural frequency and the damping ratio. To continue the analogy, an underdamped door closer would close quickly, but would hit the door frame with significant velocity, or would oscillate in the case of a swinging door.

Un-damping ($\zeta = 0$)

The system oscillates at its natural resonant frequency ω_0.

B. Rayleigh Damping

Rayleigh damping is viscous damping that is proportional to a linear combination of mass and stiffness. The damping matrix C is given by:

$$[C_R] = \alpha_R[M] + \beta_R[k] \qquad \text{(eq B.1)}$$

where M, K are the mass and stiffness matrices, respectively and α_R, β_R are constants of proportionality.

Rayleigh damping does afford certain mathematical conveniences and is widely used to model internal structural damping. One of the less attractive features of Rayleigh damping is that the achieved damping ratio varies as response frequency varies. The stiffness proportional term contributes damping that is linearly proportional to response frequency and the mass proportional term contributes damping that is inversely proportional to response frequency.

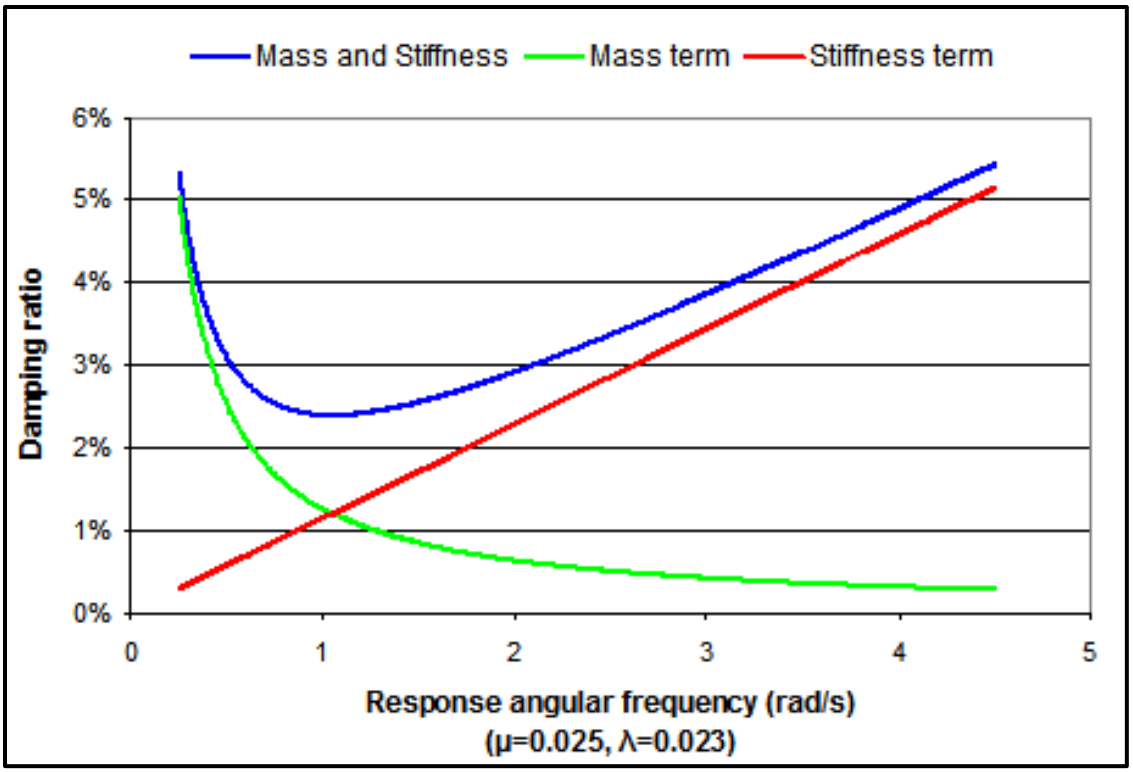

Figure C.1 Rayleigh damping ratio VS angular frequency (source: www.orcina.com)

With this formulation the damping ratio is the same for axial, bending and torsional response.

Classical Rayleigh damping results in different damping ratios for different response frequencies according to the following equation:

$$\zeta = 0.5\left(\frac{\alpha_R}{\omega} + \omega\beta_R\right) \qquad \text{(eq B.2)}$$

$\zeta\ and\ \omega$ are critical damping ratio (a value of 1 corresponds to critical damping) and angular frequency (rad/sec)

C. API Static BHA Design

1. Tension Loading

The design of the drill string for static tension loads requires sufficient strength in the topmost joint of each size, weight, grade, and classification of drill pipe to support the submerged weight of the entire drill pipe plus the submerged weight of the collars, stabilizer, and bit. This load may be calculated as shown in Equation 1. The bit and stabilizer weights are either neglected or included with the drill collar weight.

$$P = [(L_{dp} \times W_{dp}) + (L_c \times W_c)] K_b \qquad \text{(eq C.1)}$$

P = submerged load hanging below this section of drill pipe, lb.,

L_{dp} = length of drill pipe, ft.,

L_c = length of drill collars, ft.,

W_{dp} = weight per foot of drill pipe assembly in air, lb/ft.,

W_c = weight per foot of drill collars in air, lb/ft.,

K_b = buoyancy factor = $1 - \frac{\rho_m}{\rho_s}$; $\rho_{steel} = 489.5 \frac{lb}{ft^3} = 65.437 \frac{lb}{gal}$

Any body floating or immersed in a liquid is acted on by a buoyant force equal to the weight of the liquid displaced. This force tends to reduce the effective weight of the drill string and can become of appreciable magnitude in the case of the heavier muds.

The yield strength as defined in API specifications is not the specific point at which permanent deformation of the material begins, but the stress at which a certain total deformation has occurred. This deformation includes all of the elastic

deformation as well as some plastic (permanent) deformation. Safety factor of 90% is introduced as the maximum allowable load tension

$$P_a = P_t \times 0.9 \qquad \text{(eq C.2)}$$

P_a = maximum allowable design load in tension, lb.,

P_t = theoretical tension load from table, lb.,

0.9 = a constant relating proportional limit to yield strength.

The difference between the calculated load P and the maximum allowable tension load represents the Margin of Over Pull (MOP).

$$MOP = P_a - P \qquad \text{(eq C.3)}$$

The same values expressed as a ratio may be called the Safety Factor (SF).

$$SF = \frac{P_a}{P} \qquad \text{(eq C.4)}$$

The selection of the proper safety factor and/or margin of over pull is of critical importance and should be approached with caution. Failure to provide an adequate safety factor can result in loss or damage to the drill pipe while an overly conservative choice will result in an unnecessarily heavy and more expensive drill string. The designer should consider the overall drilling conditions in the area, particularly hole drag and the likelihood of becoming stuck. The designer must also consider the degree of risk which is acceptable for the particular well for which the drill string is being designed.

Normally the designer will desire to determine the maximum length of a specific size, grade and inspection class of drill pipe which can be used to drill a certain well. By combining Equation A.1 and A.3, the following equation results:

$$\frac{P_t \times 0.9 - MOP}{W_{dp} \times K_b} - \frac{W_c \times L_c}{W_{dp}} = L_{dp} \qquad \text{(eq C.5)}$$

If the string is to be a tapered string, i.e., to consist of more than one size, grade or inspection class of drill pipe, the pipe having the lowest load capacity should be placed just above the drill collars and the maximum length is calculated as shown previously. The next stronger pipe is placed next in the string and the W & L term in Equation 5 is replaced by a term representing the weight in air of the drill collars plus the drill pipe assembly in the lower string. The maximum length of the next stronger pipe may then be calculated.

2. Collapse Loading

The drill pipe may at certain times be subjected to an external pressure which is higher than the internal pressure. This condition usually occurs during the drill stem testing and may result in collapse of the drill pipe. The differential pressure required to produce collapse has been calculated for various sizes, grades, and inspection classes of drill pipe and appears in API Tables. The tabulated values should be divided by a suitable factor of safety to establish the allowable collapse pressure.

$$\frac{P_p}{SF} = P_a \qquad \text{(eq C.6)}$$

P_p= theoretical collapse pressure from tables, psi,

SF = safety factor,

P_a = allowable collapse pressure, psi.

When the fluid levels inside and outside the drill pipe are equal and provided the density of the drilling fluid is constant, the collapse pressure is zero at any depth, i.e., there is no differential pressure. If, however, there should be no fluid inside the pipe the actual collapse pressure may be calculated by the following equation:

$$P_c = \frac{L \times W_g}{19.251} \qquad \text{(eq C.7)}$$

or

$$P_c = \frac{L \times W_f}{144} \qquad \text{(eq C.8)}$$

P_c = net collapse pressure, psi,

L = the depth at which P_c acts, ft.,

W_g = weight of drilling fluid, lb/gal,

W_f = weight of drilling fluid, lb/ft^3.

If there is fluid inside the drill pipe but the fluid level is not as high inside as outside or if the fluid inside is not the same weight as the fluid outside, the following equation may be used:

$$P_c = \frac{L \times W_g - (L - Y) \times W_g{}'}{19.251} \qquad \text{(eq C.9)}$$

or

$$P_c = \frac{L \times W_f - (L - Y) \times W_f{}'}{144} \qquad \text{(eq C.10)}$$

Y = depth to fluid inside drill pipe, ft.,

W_g' = weight of drilling fluid inside pipe, lb/gal,

W_f' = weight of drilling fluid inside pipe, lb/cu ft.

D. Beams Deflections (Method of Superposition)

Euler–Bernoulli beam theory is a simplification of the linear theory of elasticity which provides a means of calculating the load-carrying and deflection characteristics of beams. It covers the case for small deflections of a beam which is subjected to lateral loads only. Additional analysis tools have been developed such as plate theory and finite element analysis, but the simplicity of beam theory makes it an important tool in the sciences, especially structural and mechanical engineering.

The Euler-Bernoulli equation describes the relationship between the beam's deflection and the applied load:

$$\frac{d^2}{dx^2}\left(EI\frac{d^2w}{dx^2}\right) = q \qquad \text{(eq D.1)}$$

The curve *w(x)* describes the deflection w of the beam at some position *x* (the beam is modeled as a one-dimensional object). *q* is a distributed load, in other words a force per unit length; it may be a function of *x*, *w*, or other variables. *E* is the elastic modulus and that I is the second moment of area. *I* must be calculated with respect to the centroidal axis perpendicular to the applied loading. For an Euler-Bernoulli beam not under any axial loading this axis is called the neutral axis.

Often, w = w(x), q = q(x), and EI is a constant, so that:

$$EI\frac{d^4w}{dx^4} = q(x) \qquad \text{(eq D.2)}$$

For more complicated situations, the deflection can be determined by solving the Euler-Bernoulli equation using techniques such as the "slope deflection method", "moment distribution method", "moment area method", "conjugate beam method", "the principle of virtual work", "direct integration", "Castigliano's method", "Macaulay's method", "Method of superposition", or the "direct stiffness method".

Method of superposition

The deflection of a spring beam depends on its length, cross-sectional area, the material, where the deflecting force is applied, and how the beam is supported.

The differential equations for a deflected beam are linear differential equations. Therefore, the slope and deflection of a beam are linearly proportional to the applied loads. This will always be true if the deflections are small and the material is linearly elastic. Therefore, the slope and deflection of a beam due to several loads is equal to the sum of those due to the individual loads.

This is a very powerful and convenient method since solutions for many support and loading conditions are readily available in various engineering handbooks. Using the principle of superposition, these solutions may be combined to obtain a solution for more complicated loading conditions.

Table D.1 Beam deflection formula for different beam types

BEAM DEFLECTION FORMULAE			
BEAM TYPE	**SLOPE AT FREE END**	**DEFLECTION AT ANY SECTION IN TERMS OF *x***	**MAXIMUM DEFLECTION**
1. Cantilever Beam – Concentrated load *P* at the free end			
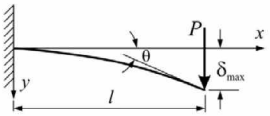	$\theta = \frac{Pl^2}{2EI}$	$y = \frac{Px^2}{6EI}(3l - x)$	$\delta_{max} = \frac{Pl^3}{3EI}$
2. Cantilever Beam – Concentrated load *P* at any point			
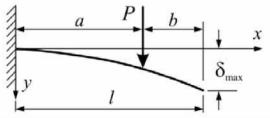	$\theta = \frac{Pa^2}{2EI}$	$y = \frac{Px^2}{6EI}(3a - x)$ for $0 < x < a$ $y = \frac{Pa^2}{6EI}(3x - a)$ for $a < x < l$	$\delta_{max} = \frac{Pa^2}{6EI}(3l - a)$
3. Cantilever Beam – Uniformly distributed load ω (N/m)			
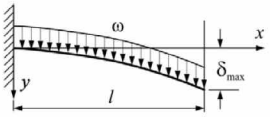	$\theta = \frac{\omega l^3}{6EI}$	$y = \frac{\omega x^2}{24EI}(x^2 + 6l^2 - 4lx)$	$\delta_{max} = \frac{\omega l^4}{8EI}$
4. Cantilever Beam – Uniformly varying load: Maximum intensity ω_o (N/m)			
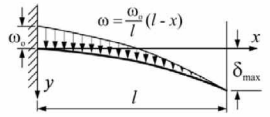	$\theta = \frac{\omega_o l^3}{24EI}$	$y = \frac{\omega_o x^2}{120lEI}(10l^3 - 10l^2 x + 5lx^2 - x^3)$	$\delta_{max} = \frac{\omega_o l^4}{30EI}$
5. Cantilever Beam – Couple moment *M* at the free end			
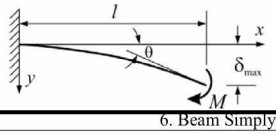	$\theta = \frac{Ml}{EI}$	$y = \frac{Mx^2}{2EI}$	$\delta_{max} = \frac{Ml^2}{2EI}$
6. Beam Simply Supported at Ends – Concentrated load *P* at the center			
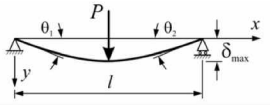	$\theta_1 = \theta_2 = \frac{Pl^2}{16EI}$	$y = \frac{Px}{12EI}\left(\frac{3l^2}{4} - x^2\right)$ for $0 < x < \frac{l}{2}$	$\delta_{max} = \frac{Pl^3}{48EI}$
7. Beam Simply Supported at Ends – Concentrated load *P* at any point			
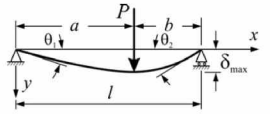	$\theta_1 = \frac{Pb(l^2 - b^2)}{6lEI}$ $\theta_2 = \frac{Pab(2l - b)}{6lEI}$	$y = \frac{Pbx}{6lEI}(l^2 - x^2 - b^2)$ for $0 < x < a$ $y = \frac{Pb}{6lEI}\left[\frac{l}{b}(x - a)^3 + (l^2 - b^2)x - x^3\right]$ for $a < x < l$	$\delta_{max} = \frac{Pb(l^2 - b^2)^{3/2}}{9\sqrt{3}\,lEI}$ at $x = \sqrt{(l^2 - b^2)/3}$ $\delta = \frac{Pb}{48EI}(3l^2 - 4b^2)$ at the center, if $a > b$
8. Beam Simply Supported at Ends – Uniformly distributed load ω (N/m)			
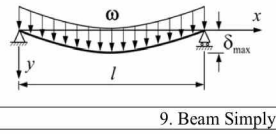	$\theta_1 = \theta_2 = \frac{\omega l^3}{24EI}$	$y = \frac{\omega x}{24EI}(l^3 - 2lx^2 + x^3)$	$\delta_{max} = \frac{5\omega l^4}{384EI}$
9. Beam Simply Supported at Ends – Couple moment *M* at the right end			
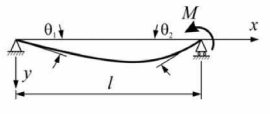	$\theta_1 = \frac{Ml}{6EI}$ $\theta_2 = \frac{Ml}{3EI}$	$y = \frac{Mlx}{6EI}\left(1 - \frac{x^2}{l^2}\right)$	$\delta_{max} = \frac{Ml^2}{9\sqrt{3}\,EI}$ at $x = \frac{l}{\sqrt{3}}$ $\delta = \frac{Ml^2}{16EI}$ at the center
10. Beam Simply Supported at Ends – Uniformly varying load: Maximum intensity ω_o (N/m)			
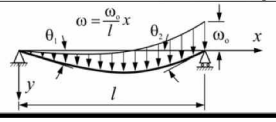	$\theta_1 = \frac{7\omega_o l^3}{360EI}$ $\theta_2 = \frac{\omega_o l^3}{45EI}$	$y = \frac{\omega_o x}{360lEI}(7l^4 - 10l^2 x^2 + 3x^4)$	$\delta_{max} = 0.00652\frac{\omega_o l^4}{EI}$ at $x = 0.519l$ $\delta = 0.00651\frac{\omega_o l^4}{EI}$ at the center

E. Finite Element Analysis

The finite element analysis (FEA) is a numerical technique for finding approximate solutions of partial differential equations (PDE) as well as of integral equations. The solution approach is based either on eliminating the differential equation completely (steady state problems), or rendering the PDE into an approximating system of ordinary differential equations, which are then numerically integrated using standard techniques such as Euler's method, Runge-Kutta, etc.

In solving partial differential equations, the primary challenge is to create an equation that approximates the equation to be studied, but is numerically stable, meaning that errors in the input and intermediate calculations do not accumulate and cause the resulting output to be meaningless. There are many ways of doing this, all with advantages and disadvantages. The Finite Element Method is a good choice for solving partial differential equations over complicated domains (like cars and oil pipelines), when the domain changes (as during a solid state reaction with a moving boundary), when the desired precision varies over the entire domain, or when the solution lacks smoothness. For instance, in a frontal crash simulation it is possible to increase prediction accuracy in "important" areas like the front of the car and reduce it in its rear (thus reducing cost of the simulation).

REFERENCES

Aburto, M. and D'Ambrosio, P. 2010. Optimizing Deepwater Salt/Subsalt Drilling with Hole Openers. *Offshore Journal* **70** (1):

Aird, P. 2009. How to Drill a Usable Hole. Kingdom Drilling, http://www.kingdomdrilling.co.uk/SectionFiles.aspx?SectionId=88&catalog=WE. Downloaded 13 May 2011.

API RP 7G, Recommended Practice for Drill Stem Design and Operating Limits, sixteenth edition. 1998. Washington, DC, USA: API.

Apostal, M.C., Haduch, G.A. and Williams, J.B. 1990. A Study to Determine the Effect of Damping on Finite-Element-Based, Forced-Frequency-Response Models for Bottomhole Assembly Vibration Analysis. SPE Paper 20458-MS presented at the SPE Annual Technical Conference and Exhibition, New Orleans, Louisiana, USA, 23-26 Spetember. doi: 10.2118/20458-MS.

Aslaksen, H., Annand, M., Duncan, R., Fjaere, A., Paez, L. and Tran, U. 2006. Integrated Fea Modeling Offers System Approach to Drillstring Optimization. SPE/IADC Paper 99018-MS presented at the SPE/IADC Drilling Conference, Miami, Florida, USA, 21-23 February. doi: 10.2118/99018-MS.

Azar, J.J. and Samuel, G.R. 2007. *Drilling Engineering,* 1st edition. Tulsa, Oklahoma, USA: PennWell Corporation.

Bailey, J.R., Biediger, E., Gupta, V., Ertas, D., Elks, W.C. and Dupriest, F.E. 2008. Drilling Vibrations Modeling and Field Validation. SPE/IADC Paper 112650-MS presented at the SPE/IADC Drilling Conference, Orlando, Florida, USA, 4-6 March. doi: 10.2118/112650-MS.

Bartko, K.M., Al-Shobaili, Y.M., Gagnard, P.E., Warlick, M. and Baim, A.S. 2009. Drill Cuttings Re-Injection (Cri) Assessment for the Manifa Field: An Environmentally Safe and Cost-Effective Drilling Waste Management Strategy. SPE Paper 126077-MS presented at the SPE Saudi Arabia Section Technical Symposium and Exhibition, Khobar, Saudi Arabia, 9-11 May. doi: 10.2118/126077-MS.

Belokobyl'skii, S.V. and Prokopov, V.K. 1982. Friction Induced Self-Excited Vibration of Drill Rig with Exponential Drag Law. *Prikladnaya Mekhankia* **18** (12): 98-101.

Besaisow, A.A., Jan, Y.M. and Schuh, F.J. 1985. Development of a Surface Drillstring Vibration Measurement System. SPE Paper 14327-MS presented at the SPE Annual Technical Conference and Exhibition, Las Vegas, Nevada, USA, 22-25 September. doi: 10.2118/14327-MS.

Besaisow, A.A. and Payne, M.L. 1988. A Study of Excitation Mechanisms and Resonances Inducing Bottomhole-Assembly Vibrations. *SPE Drilling Engineering* **3** (1): 93-101. SPE- 15560-PA. doi: 10.2118/15560-PA

Brett, J.F. 1992. The Genesis of Bit-Induced Torsional Drillstring Vibrations. *SPE Drilling Engineering* **7** (3): SPE- 21943-PA. doi: 10.2118/21943-PA

Callas, N.P. and Callas, R.L. 1980. Stabilizer Placement Series. ***Oil and Gas Journal***. **Part 1:** November 24, 1980; **Part 2:** December 1, 1980; **Part 3:** December 15, 1980; **Part 4:** December 29, 1980.

Canty, D. 2011. Field Focus: Saudi Aramco's Karan Field. Arabian Oil & Gas, http://www.arabianoilandgas.com/article-8980-field-focus-saudi-aramcos-karan-field/. Downloaded 4 July 2011.

Chen, D.C.-K. and Wu, M. 2007. Maximizing Drilling Performance with State-of-the-Art Bha Program. SPE/IADC Paper 104502-MS presented at the SPE/IADC Drilling Conference, Amsterdam, The Netherlands, 20-22 February. doi: 10.2118/104502-MS.

Compton, M., Verano, F., Nelson, G.R. and Wu, X. 2010. Managing Downhole Vibrations for Hole-Enlargement-While-Drilling in a Deepwater Environment: A Proven Approach Using Drillstring-Dynamics Model. SPE Paper 139234-MS presented at the SPE Latin American and Caribbean Petroleum Engineering Conference, Lima, Peru, 1-3 December. doi: 10.2118/139234-MS.

Craig, A.D., Hanley, C., McFarland, B., Shearer, D.R. and King, P.D. 2009. A Proven Approach to Mitigating Drilling Vibration Problems in Offshore Western Australia. IPTC Paper 13399-MS presented at the International Petroleum Technology Conference, Doha, Qatar, 7-9 December. doi: 10.2523/13399-MS.

Dareing, D.W. 1984. Drill Collar Length Is a Major Factor in Vibration Control. *SPE Journal of Petroleum Technology* **36** (4): 637-644. SPE- 11228-PA. doi: 10.2118/11228-PA

Dawson, R. and Paslay, P.R. 1984. Drill Pipe Buckling in Inclined Holes. *SPE Journal of Petroleum Technology* **36** (10): 1734-1738. SPE- 11167-PA. doi: 10.2118/11167-PA

Dupriest, F.E., Witt, J.W. and Remmert, S.M. 2005. Maximizing Rop with Real-Time Analysis of Digital Data and Mse. IPTC Paper 10607-MS presented at the International Petroleum Technology Conference, Doha, Qatar, 21-23 November. doi: 10.2523/10607-MS.

Dykstra, M.W., Chen, D.C.-K., Warren, T.M. and Azar, J.J. 1996. Drillstring Component Mass Imbalance: A Major Source of Downhole Vibrations. *SPE Drilling & Completion* **11** (4): 234-241. SPE- 29350-PA. doi: 10.2118/29350-PA

Halsey, G.W., Kyllingstad, A., Aarrestad, T.V. and Lysne, D. 1986. Drillstring Torsional Vibrations: Comparison between Theory and Experiment on a Full-Scale Research Drilling Rig. SPE Paper 15564-MS presented at the SPE Annual Technical Conference and Exhibition, New Orleans, Louisiana, USA, 5-8 October. doi: 10.2118/15564-MS.

Inglis, T.A. 1987. *Directional Drilling,* 1st edition. Norwell, Massachusetts, USA: Graham & Trotman Inc.

Jafee, A.M. and Elass, J. 2007. Saudi Aramco: National Flagship with Global Responsibilities. The James A Baker III Institute for Public Policy, Rice University, Houston, Texas, USA. http://www.rice.edu/energy/publications/docs/NOCs/Papers/NOC_SaudiAramco_Jaffe-Elass-revised.pdf

Kriesels, P.C., Keultjes, W.J.G., Dumont, P., Huneidi, I., Owoeye, O.O. and Hartmann, R.A. 1999. Cost Savings through an Integrated Approach to Drillstring Vibration Control. SPE/IADC Paper 57555-MS presented at the SPE/IADC Middle East Drilling Technology Conference, Abu Dhabi, United Arab Emirates, 8-10 November. doi: 10.2118/57555-MS.

Ledgerwood, L.W., Hoffmann, O.J.-m., Jain, J.R., Hakam, C.E., Herbig, C. and Spencer, R. 2010. Downhole Vibration Measurement, Monitoring, and

Modeling Reveal Stick/Slip as a Primary Cause of Pdc-Bit Damage in Today. SPE Paper 134488-MS presented at the SPE Annual Technical Conference and Exhibition, Florence, Italy, 19-22 September. doi: 10.2118/134488-MS.

Lin, Y.-Q. and Wang, Y.-H. 1991. Stick-Slip Vibration of Drill Strings. *Journal of Engineering for Industry* **113** (1): 38-43. doi: 10.1115/1.2899620.

Lyons, W.C. and Plisga, G.J. 2005. *Standard Handbook of Petroleum and Natural Gas Engineering,* 2nd edition. Burlington, Massachusetts, USA: Elsevier Inc.

Macpherson, J.D., Mason, J.S. and Kingman, J.E.E. 1993. Surface Measurement and Analysis of Drillstring Vibrations While Drilling. SPE/IADC Paper 25777-MS presented at the SPE/IADC Drilling Conference, Amsterdam, The Netherlands, 23-25 February. doi: 10.2118/25777-MS.

Meyer-heye, B., Reckmann, H. and Ostermeyer, G.-P. 2011. Underreamer Dynamics. SPE Paper 139893-MS presented at the SPE/IADC Drilling Conference and Exhibition, Amsterdam, The Netherlands, 1-3 March 2011. doi: 10.2118/139893-MS.

Millheim, K., Jordan, S. and Ritter, C.J. 1978. Bottom-Hole Assembly Analysis Using the Finite-Element Method. *SPE Journal of Petroleum Technology* **30** (2): 265-274. SPE- 6057-PA. doi: 10.2118/6057-PA

Millheim, K.K. 1978-1979. Directional Drilling Series. ***Oil and Gas Journal***. **Part 1:** November 6, 1978; **Part 2:** November 20, 1978; **Part 3:** December 4, 1978; **Part 4:** December 18, 1978; **Part 5:** January 1, 1979; **Part 6:** January 15, 1979; **Part 7:** January 29, 1979; **Part 8:** Februrary 12, 1979.

Palmov, V.A., Brommundt, E. and Belyaev, A.K. 1995. Stability Analysis of Drillstring Rotation. *Dynamics and Stability of Systems Journal* **10** (2): 99-110.

Payne, M.L. 1992. Drilling Bottom Hole Assembly Dynamics. PhD dissertation, Rice University, Houston, Texas, USA. http://scholarship.rice.edu/handle/1911/19083

Piersol, A.G. and Paez, T.L. 2010. *Harris' Shock and Vibration Handbook,* 6th edition. New York, New York, USA: McGraw-Hill.

Rajnauth, J.J. and Jagai, T. 2003. Reduce Torsional Vibration and Improve Drilling Operations. SPE Paper 81174-MS presented at the SPE Latin American and Caribbean Petroleum Engineering Conference, Port-of-Spain, Trinidad and Tobago, 27-30 April. doi: 10.2118/81174-MS.

SaudiAramco. 2010. Saudi Aramco Annual Review 2010. Saudi Aramco, Dhahran, Saudi Arabia. http://www.saudiaramco.com/content/dam/Publications/Annual Review/SA Annual Review 2010_modified_060811-2.pdf

SereneEnergy. 2010. Directional Control with Rotary Assemblies. Serene Energy, http://www.sereneenergy.org/Control-with-Rotary-Assemblies.php. Downloaded 3 May 2011.

Short, J.A. 1993. *Introduction to Directional and Horizontal Drilling,* 1st edition. Tulsa, Oklahoma, USA: PennWell Publishing Company.

Shuttleworth, N.E., Van Kerkoerle, E.J., Folmer, D.R. and Foekema, N. 1998. Revised Drilling Practices, Vss-Mwd Tool Successfully Addresses Catastrophic Bit/Drillstring Vibrations. SPE/IADC Paper 39314-MS presented at the SPE/IADC Drilling Conference, Dallas, Texas, USA, 3-6 March. doi: 10.2118/39314-MS.

Walker, B.H. 1986. Factors Controlling Hole Angle and Direction. *Journal of Petroleum Technology* **38** (11): 1171-1173. SPE- 15963-PA. doi: 10.2118/15963-PA

Zamudio, C.A., Tlusty, J.L. and Dareing, D.W. 1987. Self-Excited Vibrations in Drillstrings. SPE Paper 16661-MS presented at the SPE Annual Technical Conference and Exhibition, Dallas, Texas, USA, 27-30 September. doi: 10.2118/16661-MS.

VITA

Ziad A Alabdullatif was born in Riyadh, Saudi Arabia on July 27, 1984. After completing high school at Al-Manarat High School, Madinah, Saudi Arabia, in June 2002, he enrolled in the College Preparatory Center at Saudi Aramco for 1 year before enrolling in King Fahd University of Petroleum & Minerals in September 2003. He received the degree of Bachelor of Science in Petroleum Engineering from King Fahd University of Petroleum & Minerals in June 2007. During the following years, he was employed as a Petroleum Engineer at Saudi Aramco. In August 2009, he attended the Graduate School at The University of Texas at Austin where he majored in Petroleum and Geosystems Engineering.

Permanent Address: PO BOX 9118
Saudi Aramco
Dhahran 31311
Saudi Arabia

This thesis was typed by the author.